Roads, J. et al. 2008: GEWEX Water and Energy Budget Study. Earth Interactions (submitted)

GEWEX Water and Energy Budget Study

J. Roads, E. Bainto
Experimental Climate Prediction Center
Scripps Institution of Oceanography, UCSD
La Jolla, CA 92023
jroads@ucsd.edu

K. Masuda
Frontier Research Center for Global Change
Japan Agency for Marine-Earth Science and Technology
3173-25 Showa, Kanazawa-ku, Yokohama 236-0001, Japan
masuda@jamstec.go.jp

M. Rodell
Hydrological Sciences Branch, Code 614.3
NASA Goddard Space Flight Center
Greenbelt, MD 20771
Matthew.Rodell@nasa.gov

W. B. Rossow
CREST at The City College of New York
Steinman Hall (T-107)
New York, NY 10031
wbrossow@ccny.cuny.edu

Corresponding Author: J. Roads
Submitted: Oct. 4, 2007
In revised form: Feb. 15, 2008

Abstract

Closing the global water and energy budgets has been an elusive Global Energy and Water-cycle Experiment (GEWEX) goal. It has been difficult to gather many of the needed global water and energy variables and processes, although, because of GEWEX, we now have globally gridded observational estimates for precipitation and radiation and many other relevant variables such as clouds and aerosols. Still, constrained models are required to fill in many of the process and variable gaps. At least there are now several atmospheric reanalyses ranging from the early NCEP/NCAR and NCEP/DOE reanalyses to the more recent ERA40 and JRA-25 reanalyses. Atmospheric constraints include requirements that the models' state variables remain close to in situ observations or observed satellite radiances. This is usually done by making short-term forecasts from an analyzed initial state; these short-term forecasts provide the next guess, which is corrected by comparison to available observations. While this analysis procedure is likely to result in useful global descriptions of atmospheric temperature, wind and humidity, there is no guarantee that relevant hydroclimate processes like precipitation, which we can observe and evaluate, and evaporation over land, which we cannot, have similar verisimilitude. Alternatively, the Global Land Data Assimilation System (GLDAS), drives uncoupled land surface models with precipitation, surface solar radiation, and surface meteorology (from bias-corrected reanalyses during the study period) to simulate terrestrial states and surface fluxes. Further constraints are made when a tuned water balance model is used to characterize the global runoff observational estimates. We use this disparate mix of observational estimates, reanalyses, GLDAS and calibrated water balance simulations to try to characterize and close global and terrestrial atmospheric and surface water and energy budgets to within 10-20% for long term (1986-1995), large-scale global to regional annual means.

1. Introduction

Closing atmosphere and surface water and energy budgets was one of the goals of the previous Global Energy and Water-cycle Experiment (GEWEX) Hydrometeorology Panel (GHP; see Lawford et al. 2004), which was comprised of representatives from the regions formerly known as the GEWEX Continental-Scale Experiments and now known as the GEWEX Regional Hydroclimate Projects (RHPs; see Sec. 5.2). Towards this goal, a number of RHP Water and Energy Budget Studies (WEBS) were launched (e.g. Roads et al. 2003; Szeto et al. 2008) to bring together needed regional data sets and model simulations. Since those initial GHP pilot projects, there have been a number of important new global observational estimates, atmospheric reanalyses, and land data assimilation data sets that have become widely available and have provided some impetus for doing another WEBS for not only individual RHPs but also for larger regions.

The regional studies of GHP are complemented by GEWEX Radiation Panel (GRP) efforts to obtain a complete global description of the water and energy cycle. Observation-based GRP global data sets now include the: National Aeronautics and Space Administration (NASA) water VAPor Product (NVAP; Randel et al. 1996); International Satellite Cloud Climatology Project (ISCCP) cloud products (Rossow and Schiffer 1999), which also include water vapor and radiative fluxes (Zhang et al. 1995, 2004), and the Global Aerosol Climatology Project (GACP; Mishchenko et al. 2007) uncertainty; independent radiative fluxes from the Surface Radiation Budget (SRB; Stackhouse et al. 2000) project; and Global Precipitation Climatology Project (GPCP, Adler et al. 2003) precipitation. Also now available are two runoff based global data products developed by the Univ. of New Hampshire in cooperation with the Global Runoff Data

Center (GRDC; Fekete et al. 1999, 2002), as well as the Climate Prediction Center's (CPC's) Merged Analysis of Precipitation (CMAP, Xie et al. 1997) precipitation and temperature data sets and Climate Research Unit (CRU; see Brohan et al. 2006) and CPC surface air temperature global data sets. Having more than one independent set of global observation-based data sets allows some assessment of the associated uncertainty.

Information about our current ability to simulate and predict these processes is obtained by comparison of these observational based data sets to more model based output/data sets such as atmospheric reanalyses, which now include: two global reanalyses from the National Centers for Environmental Prediction / National Center for Atmospheric Research (NCEP/NCAR R1, Kalnay et al. 1996) and NCEP / Dept. of Energy (NCEP/DOE R2, Kanamitsu et al. 2002), the European Centre for Medium Range Weather Forecasts (ERA40; Uppala et al. 2005), Japanese 25 year Reanalysis (JRA25; Onogi et al. 2007) as well as output from the NASA Global Land Data Assimilation System (GLDAS; Rodell et al. 2004) - a project that contributed to the GEWEX Modeling and Prediction Panel (GMPP) Global Soil Wetness Project (GSWP; Dirmeyer et al. 2006). Since GSWP, GLDAS has now developed three new upgraded and unique LDAS simulations from the NASA Mosaic, NCEP Noah, and NCAR Common Land Model (CLM) land surface models (LSMs). All GLDAS simulations used the same observation-constrained meteorological forcing dataset from Berg et al. (2005).

The focus of this study employs global data sets is to go beyond the earlier RHP-based studies to examine larger-scale features. We have limited the present WEBS to the bulk-integrated (atmosphere and surface) water and energy budget processes, including: precipitation, vertically

integrated atmospheric moisture convergence, total evaporation (including transpiration), total runoff, vertically integrated atmospheric energy convergence, latent heat of condensation, atmospheric radiative cooling, surface radiative heating, sensible and latent heat transfer from the surface to the atmosphere, and the associated radiation fluxes. Some combination error and tendency terms are also defined, which include the ground (and ocean - vertical and horizontal) energy fluxes. Water and energy state variables include: precipitable water, terrestrial soil moisture, snow equivalent water, atmospheric sensible heat, surface air and skin temperature.

It needs to be stressed here that the chosen observational estimates, atmospheric reanalyses, and GLDAS simulations are only representative rather than fully inclusive examples of available research water and energy data sets that can be used to assess not only regional but also global water and energy budget means and uncertainties. In that regard, GSWP developed a more comprehensive set of community LDAS simulations of the surface budgets and there are a number of more comprehensive assessments for radiation, precipitation (see e.g. Schlosser and Houser 2007, Trenberth et al. 2007a,b and references therein), clouds, and aerosols currently underway.

What is perhaps unique here is our attempt to combine a relatively diverse collection of observational estimates, atmospheric reanalyses, and LDAS simulations for a global to regional assessment of our current ability to characterize, close and simulate surface and atmosphere water and energy budgets and to characterize the current uncertainty. We hope this effort provides some context for these individual assessments as well as for future assessments within individual RHP regions. We also note that there have been many previous attempts to provide

syntheses of water and energy budgets (e.g. Oki 1999, Kiehl and Trenberth 1997), but these syntheses have not really focused on the uncertainty, as we do here.

This paper is organized as follows. Section 2 describes the bulk water and energy budget processes and reservoirs. Section 3 provides some brief background on the atmospheric and land data assimilation systems. Section 4 provides some brief background on the observational estimates. Section 5 discusses our comparison protocols and regional features. Section 6 then describes characteristics of the global, ocean, and land surface and atmosphere water and energy budgets. Closure and RMS errors are discussed in Sec. 7. A summary is provided in section 8. It should be noted that this paper summarizes many additional plots of global water and energy variables, which are available for the interested reader at http://ecpc.ucsd.edu/projects/ghp/WEBS/.

2. Water and Energy Budgets

Water and energy budgets are time varying 3-dimensional relationships involving various storages and transformation processes. We take vertical mass weighted averages in the atmosphere and vertical averages in the subsurface, as well as monthly time means. Mathematical details are provided by Trenberth and Guillemot (1998), Trenberth et al. (2001) and Roads et al. (2002) It should be noted here that the tendency terms should be differences in instantaneous quantities at the beginning and end of the chosen time average, although these are usually approximated from interpolations of the monthly averages; in any event the tendency terms are usually small and for the purposes of this paper, which is focused on annual mean, negligible; if we were to consider seasonal variations then seasonal tendencies in soil moisture

and ocean heat storage would be important contributors. To summarize we focus here on annual mean 2-dimensional horizontal hydroclimatic variations for the atmosphere and surface.

2.1 Water

Consider first the atmospheric and surface water mass conservation equations:

Atmospheric Water

$\partial Q/\partial t = E-P+MC+EQ'$

Surface Water

$\partial W/\partial t = P-E-N+EW'$

The two state variables for these water mass conservation equations are Q, the vertically (pressure mass weighted) integrated specific humidity or precipitable water, and W, the vertically integrated (2 meters below the surface to the surface is used here) soil moisture (M) plus snow equivalent liquid water (S). The partial derivatives indicate that these equations refer to values at a single grid point. Under suitable conditions, liquid and solid water evaporate (E) from the ocean and land surface (which includes bare soil, snow and vegetation) into the atmosphere. Water vapor is then transported by atmospheric winds to other regions, and the convergence of this moisture, MC, will increase atmospheric water vapor, Q, over some regions while decreasing Q over other regions. When Q is increased beyond the local saturation point, it condenses onto aerosols as cloud particles, which grow by condensation and coalescence and by accretion into large liquid and solid drops, which then fall as precipitation, P, to the surface. If there is no horizontal cloud water advection in a vertical atmospheric column, then the net amount of water condensed is precipitated. Although the contribution of cloud water and

precipitation particle evaporation to the total moisture budget is thought to be small, this process could be important for influencing the dynamics and models now take into account at least the evaporation of rain through unsaturated layers; in fact, most models now include a liquid cloud water equation (which is ignored here).

Surface terrestrial water (W=soil and vegetation moisture, M, + snow, S) is eventually increased by P, and M is increased through snow melt and liquid water infiltration into the soil and plants and then subsequently decreased again by evaporation, E. Excess surface water is transported to river catchments, which in turn transport the water to other locations; the net divergence of this streamflow, or runoff, N, will increase surface water in low lying regions before discharging it into the oceans; most large and regional-scale atmospheric models currently simplistically assume that excess surface water is discharged immediately to the oceans.

The surface water, W=M+S, is really only defined over land here. However, we can define a freshwater budget for the entire ocean by recognizing that there is always as much surface water leaving the land as enters the ocean. A bulk ocean freshwater budget equation can thus be written the same as above except for a change in sign in front of *N;* note that because $A_o N_o = A_L N_L$, where A_o is the area of the ocean and A_L is the area of the land; because of its larger area, the average ocean runoff is smaller than the average land runoff. There is also another approximation here in that Antarctica is not simulated by GLDAS, and thus Antarctic is not included in the land average. We estimate that this is a small error since including or omitting Antarctica changes the average runoff by less than .1 mm/day. Other land averaged processes and variables have smaller differences.

It should be noted that for a global long-term average in steady state, there is as much water precipitated as evaporated and there is as much atmospheric water converged over the land from the ocean as is discharged back to it by various rivers and streams.

The EQ' and EW' terms are part of the designated closure error terms and are described below in section 2.3.

2.2 Energy

Consider next the atmospheric and surface energy equations. The atmospheric energy equation, is derived by combining the mass weighted thermodynamic equation with the kinetic energy equation and was described previously in mathematical form by Yu et al. (1999), Trenberth et al. (2001, 2002), and Roads et al. (2002), among others:

Atmospheric Energy

$Cp\ \partial T/\partial t = SH+LP+EC+QR+ET'$

The surface energy equation is simply the surface thermodynamic equation:

Surface Energy

$C\ \partial Ts/\partial t = QRS-LE-SH+EG'$

It should be noted here that a more accurate energy equation for the atmosphere also includes a surface pressure interaction term with the orography in the tendency term, which Trenberth et al.

(2002) showed was negligible. Yu et al. and (1999) and Roads et al. (2002) also ignored the kinetic energy transport as a small term, but Trenberth et al. (2002) showed that at certain times and places (winter storm track region), kinetic energy, while small, could also be considered in the diagnostic energy transport term. Trenberth et al. (2003a,b) subsequently indicated, however, that kinetic energy was probably still a relatively small term in comparison to the sensible and potential energy transports. Still, since as shall be shown later, we do implicitly include kinetic energy flux convergence, when we deduce the energy convergence, EC, from the other physical terms, and in many locations this residual calculation for the energy flux convergence does appear to be more accurately related to the net radiation than our attempts to derive the static energy flux convergence (sensible heat +potential energy) from infrequent temporal output winds, temperatures, and geopotentials from two of the atmospheric reanalyses.

We now briefly describe more of the energy equations used here. Radiative energy input to the atmosphere consists of a small absorbed fraction of the incoming solar radiation and the difference of the net infrared radiation from the surface and the outgoing infrared radiation at the top of the atmosphere; the total is a net radiative cooling, QR (a negative quantity). The net radiant energy that reaches the surface, QRS (a positive quantity), is the source that controls the surface skin temperature, Ts, and drives evaporation. The energy convergence, EC, which is mostly a combination of sensible heat and geopotential convergence, acts to balance the net atmospheric radiation by transporting energy from warm tropical regions to cooler polar regions. EC also acts to redistribute the latent heat released into the atmosphere (LP), especially in the tropical regions. Cooling of the surface, and heating of the atmosphere by turbulent transfers of sensible heat, SH, and latent heat, LE, in the planetary boundary layer, is also governed by the

latent heat release since moist regions release more latent heat and thus require less sensible heat to achieve an energy balance. The surface skin temperature, Ts, is also influenced by transfer of heat from below the surface; this vertical transfer modulates the upper level skin temperature, which is being strongly forced by diurnal to interannual variations in the surface radiation and turbulent fluxes into the atmospheric boundary layer. This contribution has been included in the EG' term, as are the flux convergences by the ocean currents and will be discussed later in sec. 2.3.

Changes in the water phase have a profound influence on the atmospheric and surface energy. Water cools its surroundings as snow is converted to liquid and liquid and solid water are converted into water vapor, LE. Globally averaged, this latent cooling of the surface is balanced by the latent heat released in the atmosphere when water vapor is converted to liquid or cloud particles, LC (LC=LP is assumed here and includes not only condensation, but also cloud and precipitation evaporation), which helps to balance the net radiative cooling of the atmosphere, QR, as well as the SH input. The latent heat of fusion complicates this simplified picture, as does the temperature dependency of the latent heat of condensation; these complications are subsumed into the ET' and EG' terms to be described later.

The latent heat required to melt snow should be balanced by the latent heat released when snow is formed initially, but this relationship is not present in some atmospheric models; in the R1 and R2, snow at the surface is assumed when the temperature above the surface reaches a certain minimum. Similarly when water vapor is converted to snow or cloud liquid droplets are converted to snow, additional latent heating should in principle occur; however, the latent heat of

fusion is usually only included only in the surface melt process. These frozen water complications are assumed to be small contributors to the large-scale averages considered here and are also absorbed into the EG' term and ET' terms.

It should also be noted that, on the average there is as much net radiation out the top of the atmosphere as is received in the form of horizontal sensible, potential (and in some places kinetic) and latent heat flux convergence from the atmosphere (LMC+EC) and ocean (EG'). This relation incorporates the solar heating of the surface and subsequent exchanges of sensible latent heat into the local balance, so that the remaining local imbalance is equal to the horizontal flux convergence. Multiplying the water vapor equations by the latent heat of condensation and adding it to the atmospheric and surface energy equations, the total (approximate) atmosphere and surface energy equation becomes:

$$\partial(\mathrm{CpT+LQ+CTs})/\partial\mathrm{T} = (\mathrm{EC+LMC\_-NR^0})+\mathrm{EG'} + (\mathrm{ET'+LEQ'})$$

Again, this total energy budget equation is derived by adding the surface energy and the atmospheric energy equations together and then also adding in the latent energy by multiplying the precipitable water equation by the latent heat of condensation, which then removes the precipitation and evaporation terms. The total energy thus includes the dry (static+geopotential+kinetic) and moist atmospheric energy (EC+LMC) as well as the energy flux convergences associated with the land and ocean (EG'). The atmospheric total energy flux convergences, (EC+LMC) balance the net radiation at the top of the atmosphere, NR^0 over land

and over the ocean, EG', which includes ocean energy flux convergences, also makes a major contribution in many places.

The radiation budget is described below. Please note that the atmosphere radiative cooling (QR) is simply the difference between the net radiation flux at the surface and the top of atmosphere (NR^1-NR^0), and that the surface radiative heating is simply the negative of the net radiation flux at the surface (-NR^1 =QRS).

Atmosphere Radiation budget

$QR = NR^1-NR^0 = (USW^1-DSW^1)+((ULW^1-DLW^1) -(USW^0-DSW^0)-((ULW^0)$

Surface Radiation Budget

$QRS = -NR^1 = -(USW^1-DSW^1)-((ULW^1-DLW^1)$

Here, USW is the upward or reflected solar radiation at the surface, superscript 1, or top of atmosphere, superscript 0. DSW is the incoming radiation at either the surface or top of atmosphere depending on the superscript. ULW is either the upward surface or the outgoing longwave radiation to space, depending on the superscript. DLW is the downward longwave at the surface from the overlying atmosphere.

The closure error terms EG', ET', and EQ' are described below in section 2.3.

2.3 Closure error terms

Closure errors, EQ' and EW', can arise from errors in each of the terms. For example, it is possible to write an error budget for the atmospheric water budget as:

$$\Delta \partial Q/\partial t - \Delta E + \Delta P - \Delta MC = EQ'$$

Here the Δ indicates the difference from the true values. We assume that if correct values could be inserted into this equation, there would be no closure error. Now since the closure error is actually the combination of errors in all of the processes; this closure error could be larger than any single error, although due to perhaps fortuitous cancellations, this closure error is usually smaller than any individual process error. Still, the closure error is at least representative of the magnitude of the overall error.

Since models are designed to close budgets there should in principle be no model closure error terms; instead there should be compensating errors in all of the terms. However, atmospheric reanalysis models are continually nudged (reinitialized) toward observational estimates and this nudging results in a model increment. This model increment is the difference between the 6-hour forecast and the analysis at the same time, divided by 6 hours. As discussed by Ruane and Roads (2008a), this model increment is usually much larger than any natural tendency, which is the difference between the analyses for different initial times. Except for the global mean, we cannot easily deduce this analysis increment, which can be positive or negative depending upon season and model. Based on the global means and identification of the tendency/closure error terms

described below, we do, however, believe the increments are relatively small in comparison to larger errors in other processes.

Some additional approximations are also absorbed by the ET' and EG' closure error terms. Again, it is somewhat of an approximation to assume that latent heat released by precipitation can be simply approximated by L*P, where L is the latent heat of condensation for water changing to vapor at 0 degrees Celsius. L and has a temperature dependence as noted earlier, not to mention a dependence on how ice is involved in the conversion. Also, again EG' includes the ground heat flux that acts to heat to the surface during the colder part of the year and cool the surface during the warmer part of the year (not to mention the potential diurnal effects which are averaged out here); EG' also includes the energy used to melt snow. Also, over the ocean, EG' represents the vertically integrated horizontal heat flux convergence and seasonal heat capacity change; in some locations, this oceanic heat convergence and seasonal heat capacity change can be as large as the atmospheric heat transport (see e.g. Trenberth et al. 2001).

These closure error terms, which are at least an estimate of the magnitude of the overall error, can be combined here with the negative of the tendency terms. These combination closure /tendency error terms can then be computed as

$EQ=EQ'-\partial Q/\partial t=(P-E-MC)$

$EW=EW'-\partial W/\partial t=(E+N-P)$

$ET=ET'-Cp\partial T/\partial t=-(QR+SH+LP+EC)$

$EG=EG'-C\partial Ts/dt=-(QRS-SH-LE)$

Subtracting the tendency term from the closure error term is useful given that we do not really understand how to compute some of the tendencies, especially over the ocean where the skin temperatures are usually part of the reanalysis input, and over the land regions where the skin temperature is determined as a balance of the other terms, including the ground heat flux, which is only included here as part of EG. We can perhaps eventually deduce the magnitude of some of the monthly to seasonal tendencies from the monthly to seasonal variations in these closure error terms, so long as the budget closure errors are small in comparison to the monthly to seasonal variations, which they are in the model based data sets described below. Note that the tendency terms are presumably zero for the long-term annual means discussed in this paper but will be nonzero for seasonal variations and in some cases may be quite important in the seasonal balance. We also did not find any significant tendencies during this longer time period (1986-1995) for any of the variables, although there are certainly interannual variations that are important for establishing some uncertainty. As shall be seen, the major uncertainty arises from the different data sets rather than from the uncertainty associated with temporal variations in 10-year means.

Finally, as further discussed below, in addition to having imperfect observational estimates for many processes, some processes like land evaporation and sensible heating, we have no reliable observations. Therefore for the turbulent fluxes over land we resorted to using model based estimates for these terms.

3. Model Based Data Sets

Atmospheric analysis systems were first developed in the 50's to provide initial conditions for atmospheric weather forecasts. It was soon realized that these analyses possessed the potential capability of not only initializing the weather forecasts but also providing additional information about the corresponding physical processes since the analyses were using the best available analyzed observations and parameterizations to simulate various physical processes. Since it was difficult to use these atmospheric analyses to look at trends or even interannual variations because of constant improvements and changes in the observing systems and models being used for the first guess, reanalyses projects, whereby at least the model could be fixed for a period of time, then began (see e.g. Schubert et al. 1993, Gibson et al. 1997, Mesinger et al. 2006), and we now have several global and regional reanalyses being used for a multitude of studies.

It was subsequently realized that the near-surface (land) output of these models might be improved by using so called land data assimilation systems forced with observed precipitation, radiation, and near surface meteorological data (from reanalyses). These GLDAS simulations, which actually currently do not strictly assimilate observations, were thus developed and are included here for comparison. In addition to surface features, such as runoff, these GLDAS simulations provide an alternative estimate to atmospheric reanalyses for the surface turbulent fluxes over land.

Further details about the reanalyses and GLDAS simulations used for this study are provided below.

3.1 Reanalyses

Atmospheric and surface reanalyses provide our easiest access to information about global to regional water and energy budgets and the ones used below are described below. As noted by many authors, there are numerous problems with reanalyses (see. e.g. Bromwich et al. 2004, Bengtsson et al. 2004 and many others) and thus their results should be taken only with lots of uncertainty. For that reason we have tried to include at least 4 atmospheric reanalysis and 3 GLDAS simulations for comparison: we judge these to be representative rather than all-inclusive and as providing an estimate of current uncertainties.

3.1.1 RI

The global spectral model (GSM) used for the NCEP/NCAR Reanalysis (RI; Kalnay et al. 1996) was based upon the Medium-Range Forecast (MRF) model then used at NCEP for making the four-times-daily Global Data Assimilation System (GDAS) analysis and medium-range (6-14 day) predictions. The GSM used a primitive equation or hydrostatic system of virtual temperature, humidity, surface pressure, mass continuity, vorticity, and divergence prognostic equations on terrain- following sigma (sigma is defined as the ratio of the ambient pressure to surface pressure) coordinates. These levels (28) were concentrated near the lower boundary and tropopause. Unlike the higher resolution GDAS, RI used a horizontal resolution of T62. An innovative feature of this reanalysis was the use of a modern land surface model (OSU; Mahrt and Pan 1984), although a strongly damped nudging to an assumed climatology was required to keep the model from drying out in certain regions (Roads et al. 1999).

3.1.2 R2

An upgraded version of the NCEP GSM was used for the NCEP/DOE AMIP Reanalysis 2 (R2; Kanamitsu et al. 2002). Besides a few physical parameterization changes, a few bugs in the R1 were also fixed. R2 snow amount was prescribed from operational files instead of using a fixed climatology (which was mistakenly used in R1 for a few years). Horizontal diffusion was applied to pressure surfaces, rather than sigma surfaces, which resulted in less spectral noise in the precipitation and snowfields. The radiation was computed on the full model grid instead of a coarser grid. The cloudiness-relative humidity relationship was refined. There were some other important differences in the boundary layer. In the R1, boundary layer vertical transfer occurred via eddy diffusion coefficients having Richardson number dependence. In R2, a non-local diffusion concept was used for the mixed layer (constant diffusion coefficients were still applied above the boundary layer). Finally, unlike R1, R2 did not force the soil moisture to an assumed climatology; R2 corrected, instead, the model soil moisture by adding the previous pentad (5-day) difference (positive or negative) between the reanalysis precipitation and observed precipitation to the soil moisture or runoff.

3.1.3 ERA40

ERA40 (1957-2003) was based on the operational MRF at ECMWF (ca. 2001). Besides having the advantage of using a model with later generation physics and additional observations, ERA40 had higher resolution 60LT159 than the NCEP reanalyses (28LT62). Some of the main physics improvements of note were the addition of the new land surface parameterization of Viterbo et al. (1999), addition of an ocean wave model (Janssen et al. 2002) and major modifications to the parameterizations of deep convection, radiation and clouds (Gregory et al. 2000; Jakob and Klein

2000). A parameterization for stratospheric humidity involving methane oxidation was also added. Perhaps the most innovative aspect of ERA40 reanalysis, however, was the assimilation of numerous new satellite measurements. Reanalysis products are available from the WWW (http://www.ecmwf.int/research/era/)

3.1.4 JRA25

The latest reanalysis available at the time of this study was the Japanese 25-year ReAnalysis (JRA-25, 1979-2004, see Onogi et al. 2007), conducted by the Japan Meteorological Agency (JMA) and Central Research Institute of Electric Power Industry (CRIEPI). This reanalysis was based on the JMA global analysis, which was operational in 2004, but the horizontal resolution of the model was reduced to T106. The number of layers of the model was 40. All of the satellite measurements available to ERA-40 were also used for this latest generation product. See http://jra.kishou.go.jp.

3.2 GLDAS

GLDAS (Rodell et al. 2004) uses the Land Information System (LIS; Kumar et al., 2006) software to drive multiple, sophisticated land surface models (LSMs) offline (not coupled to the atmosphere). The LSMs are more sophisticated versions of the land models used in the reanalyses, which benefit from the GLDAS observation-based land parameter and meteorological forcing inputs. A vegetation-based approach is used to simulate sub-grid scale variability, with a 1-km global vegetation dataset as its basis. Soil and elevation parameters are based on high-resolution global datasets. Observation-based and corrected precipitation and downward radiation and output meteorological fields from global atmospheric data assimilation

systems are employed as forcing data. Several multiyear retrospective simulations at lower spatial resolutions have been executed, including one, which was specifically made available for this study. Again, these GLDAS simulations make up only a small subset of the GSWP model simulations and are thus only a representative sample of all possible LDAS simulations.

4. Observational estimates

Many of the global observational estimates came from GEWEX's attempt to develop water and energy products from gauge stations, geostationary satellite infrared and polar orbiter passive microwave observations. Each of these and other data sets is briefly described below. We designate them as observational estimates (EST1 or EST2) on the figures referring to **Table 1** for their actual designation. We use the average of EST1 and EST2 to come up with an actual EST for calculation of climatological means, standard deviations, etc.

4.1 Precipitation

One of the major goals of the Global Precipitation Climatology Project (GPCP; Adler et al. 2003, Gu et al. 2007) has been to develop a more complete understanding of the spatial and temporal patterns of global precipitation. Data from over 6,000 rain gauge stations, and satellite geostationary infrared and passive microwave observations have been merged to estimate monthly rainfall on a 2.5-degree global grid from 1979 to present. The Global Precipitation Climatology Centre maintains the collection of high quality rain gauge measurements, which are used to prepare the comprehensive land-based rainfall analyses. The combination with the satellite-based rainfall estimates provides the most complete analysis of rainfall available to date over the global oceans, and adds necessary spatial detail to the rainfall analyses over land. A

similar precipitation data set from the Climate Prediction Center (CPC) Merged Precipitation Analysis was also available (Xie and Arkin 1997). http://www.cdc.noaa.gov/cdc/data.cmap.html. There are a number of differing assumptions over the ocean and land; for example, GPCP precipitation was corrected for under-catch, especially in cold and windy areas. Yin et al. (2004) document many of the differences between these two data sets. Although we might think that precipitation data is among the most accurate of our available observational estimates, there may still be large problems with appropriate corrections to observed values, especially over cold, high elevation regions (see. e.g. Yang et al. 2005, Adam et al. 2006).

4.2 Radiation

The NASA/GEWEX Surface Radiation Budget (SRB) Project developed a 12-year surface short wave (SW) and long wave (LW) flux dataset, based on satellite observations. The SRB 2.1 monthly averages come from the NASA Langley Atmospheric Sciences Data Center on a regular global grid at 1-degree resolution, and were available to us from July 1983 to October 1995 at (http://eosweb.larc.nasa.gov). Later versions cover a longer time period. The SW and LW fluxes at the top of atmosphere and surface are derived using, respectively, Pinker and Laszlo (1992) and Fu et al. (1998) algorithms, and a parameterized model for quality control (Staylor 1985, Darnell et al. 1992) is also applied to generate the SRB output data. The cloud properties were taken from the International Satellite Cloud Climatology Project (ISCCP) DX data (Rossow and Schiffer 1999). The Goddard Earth Observing System-1 (GEOS-1) data assimilation product provided the necessary meteorological profiles. The SW and LW fluxes are originally on a 3-hourly temporal resolution and then averaged into monthly averages.

An alternative 23-year (1983-2006) global radiative flux data product (called ISCCP FD; Zhang

et al. 2004) was created by employing the NASA GISS climate GCM radiative transfer code and a collection of global datasets describing the properties of the clouds and the surface every 3 hours daily atmospheric profiles of temperature and humidity (NOAA TOVS), daily ozone abundances (TOMS), a climatology of cloud vertical layer distributions from rawinsonde humidity profiles, a climatology of cloud particle sizes, a climatology of stratospheric aerosol and water vapor (SAGE-II), a climatology of the diurnal variations of near-surface air temperature (surface weather observations and NCEP-1 re-analysis), a climatology of tropospheric aerosols (NASA GISS climate model), and the spectral dependence of land surface albedo and emissivity by land-cover type (NASA GISS climate model). Note that both of these radiative flux products have been extensively compared with ERBE/CERES and BSRN datasets (Zhang et al. 2004), showing that they are quantitatively very similar. Moreover, since the ERBE product does not provide global coverage for the whole time period, we used only these two products here.

4.3 Oceanic latent and sensible heat fluxes

Although the initial purpose of this paper was to try to identify water and energy budgets over land regions, there is some value to providing a preliminary comparison over the ocean in that it contributes to the global mean budgets. In that regard, Chou et al. (2003) derived 13.5-yr (July 1987– December 2000) dataset of daily surface turbulent fluxes over global oceans was derived from the Special Sensor Microwave Imager (SSM/I) radiance measurements. This dataset, the Goddard Satellite-based Surface Turbulent Fluxes, version 2 (GSSTF2), had a spatial resolution of 1 deg. by 1 deg. latitude–longitude and a temporal resolution of 1 day. Turbulent fluxes were derived from the SSM/I surface winds and surface air humidity, as well as the 2-m air and sea surface temperatures (SST) of the NCEP–NCAR reanalysis, using a bulk

aerodynamic algorithm based on the surface layer similarity theory. The GSSTF2 bulk flux model was compared to turbulent fluxes computed from ship data for a number of experiments. In addition, the GSSTF2 daily wind stress, latent heat flux, wind speed, surface air humidity, and SST compare reasonably well with those of the collocated measurements of many field experiments. The GSSTF2 is useful for climate studies and were submitted to the sea surface turbulent flux project (SEAFLUX) for intercomparison studies.

HOAPS-3, "Hamburg Ocean Atmosphere Parameters and Fluxes from Satellite Data" (Anderson et al. 2007), an updated version of the HOAPS 2 (Fennig et al. 2006) ocean climatology of precipitation and evaporation over the global ice-free ocean beginning Jul. 1987, has recently been released. Like the GSSTF2, HOAPS-3 uses the Special Sensor Microwave Imager (SSM/I) operating on the polar orbiting Defense Meteorological Satellites Program (DMSP) satellites to derive such fields over the ice-free global oceans. One intention during the development of HOAPS was to derive the global ocean freshwater flux consistently from one satellite based data set. Consequently, great care was put into inter-sensor calibration for homogeneous and reliable spatial and temporal coverage. Except for the SST, all HOAPS variables are derived from brightness temperatures of the SSM/I radiometers and thus these two ocean data sets, along with the reanalyses, provide some measure of our current uncertainty in the ocean fluxes.

4.4 Runoff

The Global Runoff Data Center (GRDC) collects and disseminates hydrological data to support projects within the World Climate Research Programme (WCRP) of the World Meteorological Organization (WMO) as well as for other programs. The Centre provides a mechanism for the

international exchange of data pertaining to river flows on a continuous, long-term basis. The scope of data collection is global, regional and on catchment scale. The database, which is continually updated, contains monthly discharge data information for over 2,900 hydrologic stations in river basins located in 143 countries. From this GRDC database Fekete et al. (1999, 2002) developed a global 0.5-degree climatological data set, which used discharge observations generally from the mid-1960s through the mid-1980s to calibrate a water balance model forced by Legates and Willmott (1990a,b) climatological precipitation and temperature data sets. Subsequently (Fekete et al. 2002, the Univ. of New Hampshire - Global Runoff Data Centre (UNH-GRDC) developed global monthly mean runoff fields for the ISLSCP period (Hall et al. 2006) ISLSCP data archives. These monthly water balance model estimates for the 1986-95 time period were calculated using climate forcing data (i.e. air temperature, precipitation, wind speed, cloud coverage, vapor pressure deficit) from the Climate Research Unit (CRU) of the University East Anglia (New et al. 1999 and 2000). The resulting composite runoff fields preserve the spatial patterns of the water balance model runoff and yet are constrained by the observed discharge, unlike all the other water balance models in this comparison. As such we believe these calibrated models represent our best estimates of the surface runoff for continental scale regions. In particular, this takes into account water management practices that may have dramatic impacts in certain regions. It should be noted that there have been few other attempts to develop a globally gridded data sets although there have been some attempts to provide updated estimates of the coastal runoff into the ocean (see e.g. Dai and Trenberth 2002, who used the R1 MC forcing data).

4.5 Atmospheric moisture and energy transport

Atmospheric moisture and heat transports are internally calculated as part of the global model calculations at each dynamical time step but are usually not saved and accumulated, unlike say the precipitation or radiation. There have, however, been attempts to emulate what the large-scale reanalysis models would do at the initial time step with the large-scale analyzed winds, humidities, temperatures, and geopotentials. Roads et al. (2002) described a computation using the NCEP/NCAR reanalysis and the data from that study is used here. Similar moisture and energy convergence datasets were put together for the ERA40 reanalysis. http://dss.ucar.edu/datasets/ds117.0/. (See Trenberth et al. 2007a). Although these calculations use only analyzed values every 6 hours, there is some evidence (e.g. Roads et al. 1998) to suggest that the average values do provide reasonable estimates for the observed transports and flux convergences. This is also true here although there do seem to be some exceptions, especially in high latitudes. It should be noted that the energy fluxes calculated here do not include the kinetic energy as this was originally assumed to be small. Trenberth et al. (2002) do show that at certain times and places, e.g. storm track regions during winter, kinetic energy, while small is not negligible. Trenberth and Stephaniak (2003a,b) do indicate, though, that kinetic energy is probably a relatively small contribution in most places.

Still, these moisture convergence and energy convergence calculations, while based upon analyzed observations, are model dependent, especially in the tropical regions (Roads 2003). Also, it is not clear how important the implicit and numerical horizontal diffusion may be, especially in mountainous regions. For comparison, we also decided to estimate the moisture convergence from the other atmospheric reanalysis terms via the assumed budget

$$MC = P - E + \frac{\partial Q^A}{\partial t}$$

Where $\frac{\partial Q^A}{\partial t}$ is the tendency computed from the analysis terms. The above estimate for MC then includes any model analysis increment error $\frac{\partial Q^M}{\partial t} - \frac{\partial Q^A}{\partial t}$, where $\frac{\partial Q^M}{\partial t}$ is the difference between the analysis 6 hour forecast and analysis; in other words, the increment should be separate analysis term instead being absorbed here in this residual calculation for MC.

In a similar fashion the energy convergence was estimated for all the reanalyses from

$$EC = -SH - LP - QR + Cp\frac{\partial\{T^A\}}{\partial t}$$

Again, MC and EC computed in this way also include the analysis increment. Because of this increment, global means of these MC and EC terms will not be equal to zero, as will be shown later.

Ruane and Roads (2007a,b, 2008a,b) have suggested that the moisture and energy convergence are best approximated as a residual balance from the above equations, except that the model forecast tendency should be used in place of the analysis tendency. For example, the difference between the 6 hour forecast and analysis values for the same initial time should be used along with the model evaporation and precipitation terms, which are accumulated every time step during the analysis cycle, to calculate temporally averaged moisture convergence, rather than

trying to explicitly compute moisture convergence from instantaneous winds and humidities at the infrequent analysis output times. The alternative residual reanalysis model budget estimates described above do provide some comparison for, what we call here, the two independent observational based estimates calculated using instantaneous analysis winds, temperatures, geopotentials, and humidities from the R1 and ERA40 reanalyses.

4.5 Surface Temperature

The CRU dataset consists of merged land-based 2 m temperature and ocean-based sea surface temperature anomalies, obtained from a base period 1961-1990, on a 5-degree x 5-degree grid-box. This study used revision 2, which comprised 5159 station records, of which nearly 81% had sufficient data over the base period to produce the averages, and develop the temperature anomalies for the period of 1851 to 2001 for the land areas over the world. Jones and Moberg (2003) describe an earlier version of the current gridded historical surface temperature dataset, which benefits from the improvements to the marine data described in (Rayner et al. 2003) as well as the improvements to the land data. See http://cru.uea.ac.uk/cru/data. A similar dataset (Janowiak, personal communication) was also available from the NCEP Climate Prediction Center (CPC); after some simple quality checks, this CPC data was used as a comparison to the more standard CRU data. This data set should be related to the models 2 m temperature over both land and ocean. These data sets cannot be used to assess the strongly varying surface skin temperature over land and perhaps over the ocean.

4.6 Precipitable water

The NASA Water Vapor Project (NVAP) developed a global water vapor climatology data set for the period 1986-1999 (see Randel et al. 1996). The total column (integrated) water vapor data set brought together a combination of radiosonde observations, Television and Infrared Operational Satellite (TIROS) Operational Vertical Sounder (TOVS), and Special Sensor Microwave/Imager (SSM/I) data sets. See http://eosweb.larc.nasa.gov/PRODOCS/nvap/table_nvap.html. Previous comprehensive comparisons of this data set (e.g. Trenberth et al. 2005) have suggested that over the ocean there may be some problems and over land it may be better to just use the reanalyses, because reanalyses may have superior quality controlled input of radiosonde values. ISCCP FD (defined above) also developed an alternative version of the TOVS precipitable water and also accounted for saturation in cloud layers. This ISCCP version was used for comparison to NVAP to show the amount of uncertainty in precipitable water in comparison to the available reanalyses. Again, we believe all of these products provide representative values of the uncertainty.

5. Comparisons

5.1 Protocol

After this WEBS began, it was recognized that many of the needed variables would most likely come from efforts previously initiated by the International Satellite Land Surface Comparison Project (ISLSCP) to develop research data for community use and we therefore limited our initial study to the ISLSCP II collection period (1986-1995); GSWP also covered the same time period, for the same reason. We then attempted to find the WEBS variables from several atmospheric reanalyses (R1, R2, ERA, JRA) and GLDAS model (MOS, Noah, CLM) simulations for each

variable. From these reanalyses and simulations we could define a mean atmospheric reanalysis (Rmean) and a mean GLDAS value (Gmean).

A priori, we decided that if there were no observational estimates, we would use the mean of all the reanalysis models as the 1st estimation set (Rmean) and the mean of all the land based data assimilation as the 2nd estimation set (Gmean) and then average these two estimates for the mean observational estimate. For example, over land, evaporation, sensible heating, snow, soil moisture, skin temperature and skin could only be found from Gmean or Rmean. Now, although the GEWEX RHPs were really focused on land budgets, we ultimately decided to also include ocean estimates (GSSTF2 and HOAPS-3) of turbulent heat fluxes here since they were needed to derive global budgets and also because the global and ocean budgets provided a contrast to our estimated terrestrial budgets. As shown in **Table 1**, global means of turbulent heat fluxes have the combination of HOAPS-3 over the ocean and Rmean over the land as the first observational estimate and the combination of GSSTF2 over the ocean and Gmean over the land as the 2nd observational estimate.

There were further exceptions to the above rules.

As indicated above, there were two runoff observational estimates, one that used climatological precipitation and temperature and a tuned water balance model to generate spatial maps of climatological runoff, labeled GRDC in **Table 1**, and another that used monthly precipitation and temperature and a similarly tuned water balance model to generate monthly runoff, labeled ISLSCP. The latter could have larger but unknown error for individual months but is likely to be

more accurate for the chosen temporal time averaging period, 1986-1995. Nonetheless, we think these calibrated runoff estimates are perhaps closer to the ultimate truth than are the reanalysis and GLDAS runoff estimates, which are not tuned to any available runoff observations and instead have compensating errors in precipitation, evaporation and runoff to reach a water balance.

Finally, one variable, the atmospheric sensible heat, which is the vertically integrated pressure weighted temperature multiplied by the heat capacity, was only available from ERA40 for this time period. This omission from the other reanalyses (which did have vertically integrated water vapor) was partially alleviated when we subsequently developed the Coordinated Enhanced Observing Period (CEOP) Experimental Climate Prediction Center (ECPC) reanalysis effort (see e.g. Ruane and Roads 2007a,b) for a different time period (2001-2004). Given that the variations in the climatology appear to be small, this seemed like a reasonable choice. Note that this variable would really only be needed when calculating monthly variations in the atmospheric heat transport from the reanalysis models. It was not needed here for the annual means, but we did include it to show the potential uncertainty in this quantity from different reanalyses.

In short, although we attempted to find a couple of the "best available" observational estimates for 34 vertically integrated water and energy variables and processes to compare to 4 reanalysis models and 3 GLDAS model values, we recognize that our choices are only representative and not absolutely inclusive. Nonetheless we believe that our choices are representative and the resulting ensemble envelope provides a potentially useful estimate for understanding how well

we can currently observe and simulate global and regional water and energy budgets and processes.

Table 1 summarizes what we used for these comparisons of 34 water and energy variables. **Table 2** tabulates our "best available" estimates for these 34 selected processes and variables for several large-scale regions that will be discussed below. **Table 3** provides the standard deviation of annual means associated with these estimates. Finally, **Table 4** provides an estimate of the corresponding ensemble spatial root mean square (RMS) errors in these quantities. These RMS errors are defined in section 6.

We provide only a brief overview of many plots and tables available on our WEBS WWW site http://ecpc.ucsd.edu/projects/ghp/WEBS/index.html.

5.2 Geographic maps

Fig. 1 shows the global annual 10-year mean (1986-1995) precipitation map. There are a number of large-scale features that are in common for these observational estimates and model analyses. Large precipitation is present in the tropics over the Northern Hemisphere intertropical convergence zone and in the South Pacific convergence zone. Moving poleward, one sees the subtropical desert regions of Africa, Asia, Americas. Precipitation deserts can also occur over ocean as well as land. Further poleward are the storm track precipitation regions, which are associated with the relatively warm Gulf Stream and Kuroshio. Note that GLDAS uses the observational estimates of precipitation as input whereas the atmospheric reanalyses generate precipitation as part of the analyses, which currently do not assimilate precipitation. While it is

difficult to distinguish the differences from the observed estimates (GPCP and CMAP), as well as the forcing used for the GLDAS (GMEAN), there are a number of noticeable differences among the atmospheric reanalyses. R1 has spectral noise, although it should be noted that this was subsequently corrected in R2 (not shown); ERA40 has a tropical ocean bias; JRA25 has too little precipitation over the Amazon.

5.3 Seasonal and Interannual variations

Returning to **Fig. 1**, please note the white areas, which outline the RHP regions. As described by Lawford et al. (2004), the RHPs include the former Mackenzie GEWEX Study (MAGS), GEWEX Americas Prediction Project (GAPP), Large-Scale Biosphere - atmosphere experiment in Amazonia (LBA), and La Plata Basin (LPB) over the Americas. In Europe, there is the Baltic Sea basin Experiment (BALTEX). In Asia there are the 4 GEWEX Asian Monsoon Experiment (GAME) experimental sites, including the Lena basin in Siberia (Lena), the Tibetan plateau (Tibet), the HUBEX region in eastern Asia, and the GAME Tropical (GAME-T) regions. Over Australia there is the Murray Darling Basin (MDB). The African Monsoon Multidisciplinary Analysis (AMMA) has now begun over West Africa and is represented here by the Niger River Basin. The Northern Eurasia Earth Science Partnership, covering Russian Siberia and North China was recently accepted as the newest GEWEX RHP and although the entire NEESPI area has not been included in this analysis, some aspects of its climate should be similar to the climate of the Lena and BALTEX areas. GAPP is the largest ($8x10^6$ km^2) and HUBEX is the smallest ($4x10^5$ km^2) region studied. We also include, for comparison, averages over the global land (north of 60 deg. S. lat.), global ocean, and entire globe.

Fig. 2 shows the monthly variations in precipitation over the RHPs, the entire global land region (minus Antarctica), the global ocean region, and the globe. The solid lines bracketing the global mean (average of est1 and est2) are lines+- one standard deviation for 10-year monthly means. These 10-year standard deviations were estimated by finding the standard deviation of each monthly mean, and then by assuming that each year was independent from the next, the standard deviation of 10-year monthly means becomes the standard deviation of individual monthly means divided by $10^{1/2}$. In a similar manner, the standard deviations of annual means shown in **Table 3** can be divided by $10^{1/2}$ to provide an estimate of the uncertainty in 10 year annual mean values shown in later figures. As may be seen, the observations and GLDAS models lie close to the lines, whereas the reanalysis models tend to have large and quite significant deviations, especially during the summertime. On the average, the atmospheric reanalyses tend to have more precipitation than the observations (and GLDAS, which again uses the observations to correct reanalysis based land forcing) over both land and ocean.

5.4 Regional differences

In this section, we will briefly discuss summarize of the regional differences before evaluating summary budgets for the global and global terrestrial regions, pertinent to these RHPs.

Fig. 3a shows how the annual mean 2-meter temperature, T2m, was used to order the RHP regions from the cold Lena and MacKenzie (MAGS) river basins to the hot African region of AMMA. There is not too much disagreement among the observations, reanalyses, and GLDAS simulations, although a few regions do stand out. For example, the atmospheric reanalyses' Tibetan plateau 2-meter temperatures tend to be relatively lower than the observational estimates

and GLDAS. This is somewhat surprising given that one might assume a priori that a higher resolution data set should have lower temperatures. It should be noted that we did not attempt any adjustment based on elevation differences.

Fig. 3b shows how the atmospheric precipitable water is related to T2m, although there are exceptionally dry regions like the MDB and AMMA region and an exceptionally moist HUBEX region. The reanalyses and observations are in fairly good agreement, with perhaps the major exception being the AMMA region, where the available atmospheric observations are relatively scarce and the atmospheric structure is seasonally complex.

Fig. 3c shows the difference between the 2-meter temperature, T2m, and the surface skin temperature, Ts, which only comes from the reanalysis models. It should be noted here that the two observational estimates provided here (Rmean and Gmean) are based entirely on models and show the difference between using a reanalysis versus a forced GLDAS simulation. It is perhaps a little surprising that the scatter in this surface skin-air temperature difference is relatively large in not only the reanalyses models but also the GLDAS simulations, which all have the same T2m, although this is obviously due to the myriad ways in which Ts can be computed for a large scale region comprised of bare soil, water bodies, vegetation, etc. The AMMA region has perhaps the largest differences. Further examination of the geographic maps for the annual mean, as well as DJF and JJA differences (not shown), suggests that the uncoupled GLDAS surface temperature differences are much larger than coupled reanalyses models.

Fig. 3d shows the total 2m soil moisture also varies greatly among the models. The reanalysis models have less scatter than the GLDAS model variations. In general there tends to be somewhat larger values in the colder regions than in the dry subtropical areas, then large amounts in the tropical LBA and GAME-T regions and then smaller amounts in the relatively dry AMMA region. Again, there is fairly large disagreement for the land means between the reanalyses and GLDAS simulations, which also have fairly large disagreements among them. This was previously discussed by GSWP, who suggested that seasonal variations would have better agreement than annual means.

Fig. 4a shows the annual mean precipitation is not strongly related to temperature although in general precipitation is larger in the RHP regions with higher annual mean temperatures. Exceptions to this simple picture include the semi-arid MDB and AMMA regions. Reanalyses' disagreements with the observational precipitation estimates are much larger, especially over the tropical LBA and GAME-T regions, than the differences in the observational estimates. Presumably these differences are due to the different convective parameterizations used in each reanalysis model.

Fig. 4b shows that like the precipitation, the annual mean moisture convergence, MC, increases with temperature towards BALTEX and then decreases towards MDB and then increases steeply toward the monsoon GAME Tropics before decreasing once again over AMMA. The dryer semi-arid regions tend to show the largest disagreements and in some cases explicit negative moisture convergence is indicated, which is due to inaccuracies in the explicit MC computations or from the reanalysis increments being included in the residual MC calculations. However, for the most

part the residual MC from the reanalyses and the explicit computations show comparable variations.

Fig. 4c shows that reanalyses and GLDAS disagreements are much larger for evaporation, even for the colder midlatitude regions where evaporation is relatively small and all of the input variables are relatively well observed. Unlike precipitation, there is no independent observation base, except over the ocean. In order to obtain global observational estimates, we must therefore combine the ocean observations with either the Reanalysis mean (RMEAN+HOAPS-3) or the GLDAS mean (GMEAN+GSSTF2). It should be noted that only RMEAN was available over Antarctica and was thus used in both estimates when considering global values.

Fig. 4d shows the annual mean runoff. Like moisture convergence, runoff increases with temperature toward large values in the LBA, GAME-T, except for the arid MDB and African AMMA regions. The reanalyses tend to have larger differences with each other than the more constrained GLDAS models have among themselves, although GLDAS differences are large. The biggest disagreements occur for the LBA and GAME-T regions. Note that we have included the runoff into the ocean since it is part of the bulk ocean budget. Again, even though we do not know in detail how the freshwater is being absorbed into the ocean and transported to different regions, we do know that this global terrestrial runoff will have an influence on overall global ocean salinity.

Fig. 5a shows the negative of the top of atmospheric net radiative flux, which decreases from large positive values in the cold regions to large negative values in the warm tropical regions.

Note the almost zero values associated with the cold high-elevation Tibetan plateau. These radiative fluxes are balanced by the atmospheric and surface energy convergence (sensible and potential and perhaps kinetic) plus latent heat convergence shown in **Fig. 5c** over the various regions from the reanalyses model residual computations and from our attempts to develop an approximate explicit observational estimate (R1 and ERA40) from the sensible and potential energy convergences. Note the decrease from the cold regions which are acting as energy sinks, $EC>0$ and $NR^0>0$, to the warm moist regions, which act as energy sources, $EC<0$ and $NR^0<0$. Tibet also acts as a minor heat source. The latent heat released by precipitation is a large contributor to the atmospheric energy budget in low latitudes, which means EC is strongly negative there. In higher latitudes, sensible heat and potential energy become a stronger contributor to balancing the radiative cooling. There are some disagreements with the explicitly reanalyses computations, especially over the Tibet region (this was also found by Trenberth et al. 2001 in an earlier comparison) and higher latitude regions and some of the smaller RHP regions. Given the wide discrepancies and presumably relatively small reanalysis increments, we have become even more convinced now that model budget residual estimates for EC and MC may be more reasonable than explicit EC and MC calculations from sparse temporal data.

Fig. 5b shows the annual mean surface radiative heating. Note the increase from the cold regions to the warm tropical regions. The major exception here is the BALTEX region, which has relatively low reanalysis and GLDAS values in comparison to the observational estimates. We speculate that this may be due to the influence of snow cover and clouds but this requires further investigation. Like the atmospheric radiative cooling, there are also large differences among the observations for the LBA and GAME-T regions.

Fig. 5d shows the annual mean surface turbulent heat fluxes, SH+LE. The increase in this quantity occurs mostly because of the latent heat of evaporation (not shown). Unlike the evaporation, SH does not seem to have a clear relationship to surface temperature, presumably because the latent heat of evaporation is such a strong constraint; land regions have larger values; semi arid regions, MDB AMMA have the largest values. Again, note the relatively higher values over Tibet and relatively lower values over the cloudy BALTEX region. It should be noted that ocean values, which are dominated by latent heat fluxes, have relatively large values of latent heat and taking into account the relative area of the ocean to the land, the oceans make the dominant contribution to the global water balance.

6. Water and Energy Budgets

6.1 Global Surface and Atmosphere Budgets

As shown in **Fig. 6a** and **Table 2**, on the average (annual mean, global average) the observed precipitation, which is the mean of two different observational estimates, is less than the evaporation estimated from the mean of the ocean flux data sets (HOAPS-3 and GSSTF2) combined with reanalyses or GLDAS over land. The small uncertainty about this 10-year mean has been delineated by the two horizontal lines at the observational estimate portion. The imbalance between the estimated precipitation and evaporation leads to a significant closure error, EW, EQ in the global atmospheric and surface water budgets of around 0.1 mm/day (about 3%). The reanalyses models have less of a closure error (which manifests itself in the reanalysis model calculated MC), due to compensating errors in the precipitation and evaporation fields. That is, the reanalyses tend to not only have too much evaporation; they also have too much

precipitation. Again, because of the way the model MC are calculated (as a residual of the physical terms), they have a small but nonzero MC, because of the inclusion of the analysis increment. By contrast the global MC observational estimates calculated explicitly from the reanalyses are identically zero for the global average.

There is a nonzero surface error EW, which is on the average negative for the reanalysis models, but positive for the observationally based estimates. EQ by contrast is negative, but equal in magnitude to EW, since the error equations involve the same processes for each equation. Again, please note that because of the way we compute MC from the models as a residual of the physical terms, that the model EQ closure error is zero. In any event, these closure error terms do indicate the uncertainty associated with global observational estimates. From this figure, we can say that the annual mean global precipitation and evaporation are probably 2.7 ± .1 mm/day. We probably should have higher precision since the precipitation amounts may be more accurate than the evaporation amounts. These amounts are in accordance with Schlosser and Houser (2007) and Trenberth et al. (2007a) estimates.

As shown in the global energy budget in **Fig. 6b**, on the average the net radiative cooling of the atmosphere is balanced mostly by the latent heat released by precipitation and surface sensible heating, which along with surface evaporation balance the surface radiative heating. Note that the surface closure error is negative, which could be explained by too little sensible heating, which could be related to too much evaporation. The relatively low sensible heating could also help to explain the positive error for the atmospheric energy budget. The largest model contrasts are the energy convergences. Another term with relative large variations is the sensible heat.

Note that QRS and -QR are almost equal, which they should be. Their sum is equal to the net radiation at the top of the atmosphere, which should be approximately zero for a global annual mean: in fact, the current estimates of the greenhouse forcing (i.e., net imbalance) are about 1-2 Wm^{-2} but the imbalances of the ISCCP FD and SRB products, as well as other top-of-atmosphere radiation products are a few times larger than this (cf. Zhang et al. 2004). Still, this balance is better in the observational estimate than it is in the reanalyses, which because of the sea surface temperature constraint do not have to have zero radiation balance. The individual atmospheric and surface budgets are closed within about 20 W/m**2, and the total budget to less than 10 W/m**2 which again is about 10% error. These observation error closures are comparable to the reanalysis model errors, which, again show up in the EC computations instead of in the closure errors.

To summarize (**Table 2**), on the average, atmospheric radiative cooling of about 113 W/m**2 is balanced by latent heat of condensation of about 76 W/m**2 and sensible heating of 17 W/m**2, with an estimated closure error of about 19 W/m**2. Likewise, surface radiative heating of about 117 W/m**2 is balanced by sensible heating and latent cooling of 95 W/m**2 with an estimated closure error of -22 W/m**2. Adding the two budgets results in a remarkable agreement for the total energy of -3 W/m**2. Again, the signs of the closure errors in both the atmosphere and surface energy equations suggest that the turbulent sensible heat flux estimates are underestimated.

6.2 Ocean Surface and Atmosphere Budgets

As shown in **Fig. 7a**, the observed ocean precipitation is less than the reanalyses evaporation, which it should be, of course, since moisture is transported away from the ocean to land regions. This negative moisture convergence or divergence is actually less than the estimated runoff into the ocean, which leads to a larger error, EQ, in the atmospheric water budget than in the surface water budget, EW. The atmospheric error, EQ, is presumably contributed by too much evaporation and too little moisture divergence. Note that the runoff from the reanalyses is smallest, followed by the GLDAS runoff, followed by the estimates from the water balance model. Since the reanalyses are not required to conserve water over the ocean, they end up having fairly large closure errors, EW, with the reanalyses' mean having the smallest error. The reanalysis mean does end up in many cases being the best estimate.

Fig. 7b shows the mean energy budget for the ocean regions. On the average, the atmospheric radiative cooling is mostly balanced by the latent heat of precipitation with some contribution from the surface sensible heating. Note that while the reanalyses tend to have the correct atmospheric radiative cooling, they tend to have lower values for the surface radiative heating. This allows them to have a better surface heat balance than the estimated surface heat balance, which has a closure error of about -25 W/m**2, while the atmospheric heat balance has a closure error of about 24 W/m**2.

6.3 Terrestrial Surface and Atmosphere Budgets

Fig. 8a shows the atmospheric and surface water budget terms for the entire land (terrestrial) region (minus Antarctica). Note that all of the atmospheric models tend to have too much

precipitation in comparison to observations, too much evaporation in comparison to GLDAS models, and, on the average, too little moisture convergence and runoff in comparison to observational estimates. Although reduced evaporation in the GLDAS models is balanced by increased runoff, GLDAS runoff is still, on the average, less than the observational estimates. The upshot is that we wind up having an observed closure error that is on the average about as large as the runoff. However, like the global budget, this closure error also occurs because of too much evaporation, which may explain why the closure error EQ continues to be negative and EW continues to be positive, as shown previously for the global means. **Fig. 8a** also shows that the closure error in the total budget, atmospheric plus surface, is relatively smaller than the closure error in each of the individual components, again suggesting that the individual errors are canceling. Note that the closure error in the land equation is less when using the second observation set, which includes the reduced evaporation from GLDAS. This indicates that the GLDAS may have a better approximation for the evaporation as well as the runoff.

Fig. 8b shows the mean energy budget for the global land regions. Of interest here is that the biases and uncertainties of the surface sensible and latent heat terms are likely much larger than corresponding biases and uncertainties in the radiation, precipitation, and transport terms. Again the GLDAS models tend to have biases and uncertainties comparable to the atmospheric reanalyses. Also in this case, if the sensible heating is too small then the atmospheric budget will have a positive closure error and the surface budget will have a negative closure error. Having too small a sensible heating would also be consistent with having too large an evaporation.

7. Errors

7.1 Closure

Fig. 9a shows the annual mean closure values for the surface energy budget. In general, use of GLDAS surface flux values for the estimated surface observation fluxes results in smaller values, which may be due to GLDAS models being more constrained by input observations (observed precipitation and radiation) than current atmospheric reanalyses. There are, however, some exceptions, such as the LBA region, where the observational estimates are large, although, these large variations are probably related to the relatively high surface radiative heating in the ISCCP FD in comparison to the SRB. The surface energy closure error, EG, is almost zero for all of the GLDAS models, except perhaps for Tibet.

Fig. 9b shows the annual mean closure errors for the surface water budget. Again, in general, using the GLDAS models' evaporation estimate results in smaller values, with the possible exception of LBA, GAME-T, and Tibet. The relatively large values here could be related to the observational estimates of runoff, which are quite high in these regions. The models on average do not simulate the large runoff, although these errors could also be related to the estimated evaporation still being too high for the GLDAS simulations as well as the reanalyses.

The closure errors for the atmospheric budgets (**Figs. 9c and 9d**) have less of a pattern since they are dependent upon not only upon evaporation and sensible heating but also the explicit calculations for the atmospheric water and energy flux convergences, which we now think potentially have large errors, at least in comparison to their corresponding residual convergences calculated from the other budget terms, especially for relatively small regions encompassing the

RHP areas; however, we did not find a clear relationship between closure error and RHP area. Note in particular, the large differences associated with Tibet in the atmospheric water equation and the large differences associated with MDB in the energy equation. Also note the larger errors in the higher latitude regions. Also note the relatively large spread among the explicit calculations, which are associated mostly with the large spread between the explicit moisture and energy flux convergences shown earlier. Interestingly, the mean of these two independent explicit calculations usually results in the smallest closure error.

7.2 Spatial RMS

Let A (g) represent the temporal mean of the estimated observation at grid point g and B (g) the temporal mean of the observations and model estimates, including the Rmean and Gmean. Then the spatial root mean square (RMS) error provides another estimate of the potential errors by

$$RMS_m = (\sum_{g=1}^{G} w(g)(B_m - A)^2)^{1/2}$$

The weighted (on the Gaussian grid, w varies like the cosine of the latitude) summation is over grid points for each region and the weights sum to 1, that is, $\sum_{g=1}^{G} w(g) = 1$

Figs. 10, 11 show examples of the spatial RMS for atmospheric and surface energy terms for the various regions. The spatial RMS is larger than the bias error associated with the individual means, but still somewhat comparable and most likely our best estimate of the actual errors in the water and energy budgets. For the most part the ensemble means (Rmean and Gmean) have

the smallest errors with respect to the observational estimates, we perhaps trust most, such as radiation and precipitation and perhaps even runoff. Note, for example, note the relatively large errors in the top of atmosphere radiation (**Fig. 10**) for the reanalysis models in tropical regions as well as for the global, land, and ocean values. Note also the relatively large errors in the precipitation (**Fig. 10**) from the reanalysis models in comparison to the observations. It should be noted here that the GLDAS models have small precipitation errors since they use a forcing data set (R1) corrected with observed precipitation (GPCP). In a similar manner, the net incoming radiation at the surface is also corrected, but the GLDAS models have just as large RMS errors for the QRS terms as the reanalysis models. Again, the RMS is largest in the atmospheric water and energy flux convergences, which again, may be better estimated by residual calculations from the other physical terms in the models.

Table 4 summarizes the RMS values. In this case we only provide a total ensemble summation, which includes each observational estimate (if available), each atmospheric reanalysis and each GLDAS simulation (if available). We also include Rmean and Gmean. That is:

$$RMS3 = (\frac{1}{M}\sum_{m=1}^{M}\sum_{g=1}^{G} w(g)(B_m - A)^2)^{1/2}$$

where M is the number of ensemble members being considered. The values in **Table 4** are most likely an overestimate of our potential errors in observing and simulating the various quantities since this table mixes observational and model based estimates, but **Table 4** does provide another assessment and a companion error table to **Tables 2 and 3** that augments the simple closure error estimates, which may be underestimates of our current uncertainty due to various

cancellations among the other budget variables. In brief, except for energy convergence, most energy processes have values comparable to the maximum closure errors of 20 W/m^2 and except for moisture convergence; most water mass products have values comparable to .5 mm/day and larger. These values are relatively small for precipitation and radiation but quite large for runoff, moisture and energy convergences, and sensible heating which again have errors comparable in magnitude to their mean values. Developing better estimates for these secondary terms in the water and energy budgets are key to improving our current water and energy budgets and closure errors.

8. Summary

This study made use of observationally based estimates developed by GEWEX and other global communities as well as products from a representative ensemble of current global atmospheric and land reanalyses efforts in order to characterize the means and uncertainty in simplified bulk-integrated (atmosphere and surface) water and energy budget variables. Variables shown or tabulated included: precipitable water, terrestrial soil moisture, snow equivalent water, atmospheric sensible heat, surface air and skin temperature, precipitation, vertically integrated moisture convergence, evaporation, runoff, vertically integrated energy convergence, latent heat of condensation, atmospheric radiative cooling, surface radiative heating, and sensible and latent heat transfers from the surface to the atmosphere. In particular, this WEBS compared NVAP and ISCCP FD water vapor, SRB and ISCCP FD radiation, GPCP and CPC precipitation, GRDC and ISLSCP runoff, CRU and CPC surface temperature, and HOAP-3 and GSSTF2 turbulent fluxes, four recent atmospheric reanalysis data sets NCEP (R1 and R2), ECMWF (ERA40), and JMA (JRA25) and three GLDAS simulations, NASA Mosaic, NCEP Noah, and NCAR CLM.

It was demonstrated that for the surface terms, the most constrained system, the simulations from the GLDAS, probably had slightly better analyses over land for many of the surface water and energy terms, in that the closure error was smaller when using these estimates for the observed land surface fluxes. It is interesting, however, that the improvements were perhaps smaller than we might have anticipated (Qu and Henderson Sellers 1998) a priori, that the spread among the reanalyses models was only slightly larger than the corresponding spread among the GLDAS simulations and that the GLDAS 2 m and surface skin temperature differences were quite different from those in the coupled reanalyses. This indicates that current GLDAS simulations might be improved by moving toward more coupled systems while the reanalyses should be moving toward more constrained systems (i.e. by including observed precipitation, as for example was done for the recent North American Regional Reanalysis. (See Mesinger et al. 2006 and Nigam and Ruiz-Barradas 2006). It should also be noted that some of the observations as well as constrained atmospheric and land based analyses seemed to have larger errors than we might have anticipated a priori, indicating that more efforts are needed to observe as well as simulate water and energy budgets.

Despite various errors, our anticipated theoretical characterization of the global water and energy cycle could still be readily discerned from available observation and model based data/output. On the average, atmospheric precipitation is balanced with surface evaporation; water vapor convergence over land is balanced by outgoing streamflow to the ocean. On the average, net radiation at the top of the atmosphere is balanced by net transport of energy; net surface radiative heating over land is balanced by the net turbulent transport of energy back to the atmosphere;

atmospheric radiative cooling is balanced by the latent heat of condensation associated with precipitation, the sensible heat transport from the surface and the transport of energy from other regions. In addition, it was clear that the terms in the budgets were quite different depending upon the RHP. For example, low latitude RHPs with relatively warm annual mean climates are energy source regions whereas high latitude RHPs with relatively cold climates are energy sink regions. Despite the observational estimates and model based atmospheric reanalyses and GLDAS data sets showing these characteristic features, they do so with a 10-20% closure error for annual means and even larger closure errors for individual regions. RMS errors for 10-year means are even larger and presumably even larger errors occur for shorter (monthly) time scales. Much more work is certainly needed to continue to accurately develop all of the appropriate WEBS data sets and to further reduce perceived errors in global and regional atmospheric, ocean, and land water and energy budgets.

Acknowledgements

This research was mostly funded by NASA grants to individual investigators working on the NASA NEWS project. Grants include NASA-NNG05GR40G to J. Roads and NASA NNXD7AO90G to W.B. Rossow. We thank the following individuals for their help and guidance: R. Adler and G. Huffman for GPCP, P. Arkin and P. Xie for CMAP, W. Ebisuzaki for R1 and R2, C. Vorosmarty, B. Fekete, and E. Douglas for GRDC and ISLSCP runoff, J. Janowiak for CPC temperature, A. Ruane for ECPC CEOP analysis, A. Beljaars for ERA40 and NCAR archival of ERA40 analyses. We thank all of the other unnamed individuals and institutions that have continued to work to provide free and open access to all of the GEWEX

and other global data and model output used for this WEBS. Comments by the anonymous reviewers helped to improve the presentation of this work.

References

Adam, J. C., E. A. Clark, D. P. Lettenmaier and E. F. Wood, 2006: Correction of global precipitation products for orographic effects. *J. Climate*, **19**(1), 15-38. doi:10.1175/JCLI3604.

Adler, R. F., and Coauthors, 2003: The Version 2 Global Precipitation Climatology Project (GPCP) Monthly Precipitation Analysis (1979-Present*). J. Hydrometeor*., **4**, 1147-1167.

Andersson, A., S. Bakan, K. Fennig, H. Grassl, C. Klepp, and J. Schulz, 2007: Hamburg Ocean Atmosphere Parameters and Fluxes from Satellite Data - HOAPS-3 - monthly mean. World Data Center for Climate. doi: 10.1594/WDCC/HOAPS3_MONTHLY.

Bengtsson, L., S. Hagemann, and K. I. Hodges, 2004: Can climate trends be calculated from reanalysis data? *J. Geophys. Res*., **109**, D11111, doi:10.1029/2004JD004536.

Berg A. A., J. S. Famiglietti, M. Rodell, R. H. Reichle, U. Jambor, S. L. Holl, and P. R. Houser, 2005: Development of a hydrometeorological forcing data set for global soil moisture estimation, *Int. J. Climatol*., **25** (13), 1697-1714.

Brohan, P., J. J. Kennedy, I. Harris, S. F. B. Tett and P. D. Jones, 2006: Uncertainty estimates in regional and global observed temperature changes: a new dataset from 1850. *J. Geophys. Res.,* **111**, D12106, doi:10.1029/2005JD006548.

Bromwich, D. H., and R. L. Fogt, 2004: Strong trends in the skill of the ERA-40 and NCEP-NCAR reanalyses in the high and midlatitudes of the Southern Hemisphere, 1958-2001. *J. Climate*, **17**, 4603-4619.

Chou, S. -H., E. Nelkin, J. Ardizzone, R. Atlas, and C. -L. Shie, 2003: Surface turbulent heat and momentum fluxes over global oceans based on the Goddard satellite retrievals, version 2 (GSSTF2). *J. Climate*, **16**, 3256-3273.

Dai, A., and K. E. Trenberth, 2002: Estimates of Freshwater Discharge from Continents: Latitudinal and Seasonal variations. *J. Hydrometeor.* **3**(6), 660.

Darnell, W. L., W. F. Staylor, S. K. Gupta, N. A. Ritchey, and A. C. Wilber, 1992: Seasonal Variation of Surface Radiation Budget Derived from International Satellite Cloud Climatology Project C1 Data. *J. Geophys. Res.,* **97**(D14), 15741-15760.

Dirmeyer, P. A., X. Gao, M. Zhao, Z. Guo, T. Oki, and N. Hanasaki, 2006: GSWP-2, Multimodel Analysis and Implications for our Perception of the Land Surface. *Bull. Amer. Soc*., **84**, 1381–1397.

Fekete, B. M., C. J. Vörösmarty, and W. Grabs, 1999: Global, Composite Runoff Fields Based on Observed River Discharge and Simulated Water Balances, GRDC Report 22, Global Runoff Data Center, Koblenz, Germany.

Fekete, B. M., C. J. Vörösmarty, and W. Grabs, 2002: High-resolution fields of global runoff combining observed river discharge and simulated water balances. *Global Biogeochem. Cycles*, **16**(3), doi:10.1029/1999GB001254.

Fennig, K., S. Bakan, H. Grassl, C. Klepp, J. Schulz, 2006: Hamburg Ocean Atmosphere Parameters and Fluxes from Satellite Data - HOAPS II - monthly mean. World Data Center for Climate. doi:10.1594/WDCC/HOAPS2_MONTHLY.

Fu, Q., P. Yang, and W. B. Sun, 1998: An Accurate Parameterization of the Infrared Radiative Properties of Cirrus Clouds for Climate Models. *J. Climate*, **11**, 2223-2237.

Gibson J. K., P. Kållberg, S. Uppala, A. Hernandez, A. Nomura, and E. Serrano, 1997: ECMWF

re-analysis project report series, 1: ERA description. ECMWF, Reading, UK.

Gregory, D., J. -J. Morcrette, C. Jakob, A. C. M. Beljaars, and T. Stockdale, 2000: Revision of convection, radiation and cloud schemes in the ECMWF Integrated Forecasting System. *Q. J. R. Meteorol. Soc*., **126**, 1685-1710.

Gu, G., R. F. Adler, G. J. Huffman, and S. Curtis 2007: Tropical Rainfall Variability on Interannual-to-Interdecadal and Longer Time Scales Derived from the GPCP Monthly Product, *J. Climate*, **20**, 4033- 4046, doi: 10.1175/JCLI4227.1.

Hall, F. G., and Coauthors, 2006: ISLSCP Initiative II global data sets: Surface boundary conditions and atmospheric forcings for land-atmosphere studies, *J. Geophys. Res.*, **111**, D22S01, doi:10.1029/2006JD007366.

Jakob, C. and S.A. Klein, 2000: A parameterization of cloud and precipitation overlap effects for use in general-circulation models. *Q. J. R. Meteorol. Soc.,* **126**, 2525-2544.

Janssen, P. A. E. M., J. D. Doyle, J. Bidlot, B. Hansen, L. Isaksen and P. Viterbo, 2002: Impact and feedback of ocean waves on the atmosphere. *In Advances in Fluid Mechanics, Atmosphere-Ocean Interactions*, **I**, 155-197.

Jones, P. D., and A. Moberg, 2003: Hemispheric and large-scale surface air temperature variations: An extensive revision and an update to 2001. *J. Climate*, **16**, 206-223.

Kalnay, E., and Coauthors, 1996: The NCEP/NCAR 40-year reanalysis project. *Bull. Amer. Meteor. Soc*., **77**, 437-471.

Kanamitsu, M., W. Ebisuzaki, J. Woollen, S. -K. Yang, J. J. Hnilo, M. Fiorino, and G. L. Potter, 2002: NCEP-DOE AMIP-II reanalysis (R-2). *Bull. Amer. Meteor. Soc*., 83, 1631-1643.

Kiehl, J. T., and K. E. Trenberth, 1997: Earth's annual global mean energy budget. *Bull. Amer. Meteor. Soc.*, **78**, 197-208.

Kumar, S. V., and Coauthors, 2006: Land Information System - An interoperable framework for high resolution land surface modeling. *Environ. Modelling and Software*, **21**, 1402-1415.

Lawford, R.G., and Coauthors, 2004: Advancing Global-and Continental-Scale Hydrometeorology: Contributions of GEWEX Hydrometeorology Panel. *Bull. Amer. Meteor. Soc*., **85**, 1917–1930.

Legates, D. R. and C. J. Willmott, 1990a: Mean seasonal and spatial variability in gauge-corrected, global precipitation. *J. Climatol*., **10**, 111-1271.

Legates, D. R. and C. J. Willmott, 1990b: Mean seasonal and spatial variability in global air temper. *Theor. Appl. Climatol*., **41**, 11-21.

Mahrt, L. and H. Pan, 1984: A two layer model of soil hydrology. *Boundary Layer Meteorol.,* **29***,* 1-20.

Mesinger, F., and Coauthors, 2006: North American Regional Reanalysis. *Bull. Amer. Meteor. Soc*., **87**(3), 343-360.

Mishchenko, M. I., and Coauthors, 2007: Past, present, and future of global aerosol climatologies derived from satellite observations: A perspective. *J. Quant. Spectrosc. Radiat. Trans.*, **106**, 325-347.

New M., M. Hume and P. Jones, 1999: Representing Twentieth Century Space-Time Climate Variability: I. Development of a 1961-1990 Mean Monthly Terrestrial Climatology. *J. Climatol.*, **12**, 829-856.

New M., M. Hume and P. Jones, 2000: Representing Twentieth Century Space-Time Climate Variability: II. Development of 1901-1990 Monthly Terrestrial Monthly Grids of Terrestrial Surface. *J. Climatol.*, **13**, 2217-2238.

Nigam, S., and A. Ruiz-Barradas, 2006: Seasonal Hydroclimate Variability over North America in Global and Regional Reanalyses and AMIP Simulations: Varied Representation. *J. Climate*, **19**, 815-837.

Oki, T., 1999: The global water cycle. In Global Energy and Water Cycles. K. A. Browning and R. J. Gurney (Eds.) Cambridge Univ. Press, 10-29.

Onogi, K., and Coauthors, 2007: The JRA-25 Reanalysis. *J. Meteor. Soc. Japan***, 85**, 369 - 432.

Pinker, R. T., and I. Laszlo, 1992: Modeling Surface Solar Irradiance for Satellite Applications on a Global Scale. *J. Appl. Meteor*., **31**, 194-211.

Qu, W., and Coauthors, 1998: Sensitivity of Latent Heat Flux from PILPS Land-Surface Schemes to Perturbations of Surface Air Temperature. *J. Atmos. Sci.*, **55**(11), 1909-1927.

Randel, D. L., T. H. Vonder Haar, M. A. Ringerud, G. L. Stephens, T. J. Greenwald, and C. L. Combs, 1996: A New Global Water Vapor Dataset. *Bull. Amer. Meteor. Soc*., **77**, 1233-1246.

Rayner, N. A., D. E. Parker, E. B. Horton, C. K. Folland, L. V. Alexander, D. P. Rowell, E. C. Kent and A. Kaplan, 2003: Global analyses of SST, sea ice and night marine air temperature since the late nineteenth century. *J Geophys Res.*, **108**(D14), 2.1-2.22.

Roads, J.O., S-C., Chen, M. Kanamitsu, and H. Juang, 1998: Vertical structure of humidity and temperature budget residuals over the Mississippi River basin, *J. Geophys. Res*., 103, 3741-3759.

Roads, J.O., S. -C. Chen, M. Kanamitsu, and H. Juang, 1999: Surface water characteristics in NCEP global spectral model and reanalysis, *J. Geophys. Res*., **104** (D16) 19307-19327.

Roads, J., M. Kanamitsu and R. E. Stewart, 2002: CSE Water and Energy Budgets in the NCEP-DOE Reanalysis II. *J. Hydrometeor*., **3**, 227-248.

Roads, J., and Coauthors, 2003: GCIP water and energy budget synthesis (WEBS). *J. Geophys. Res.*, **108** (D16), 10.1029/2002JD002583.

Roads, J., 2003: The NCEP-NCAR, NCEP-DOE, and TRMM Tropical Atmosphere Hydrologic Cycles, *J. Hydrometeor*., **4**, 826-840.

Rodell, M., and Coauthors, 2004: The Global Land Data Assimilation System, *Bull. Amer. Meteor. Soc*., **85** (3), 381–394.

Rossow, W. B., and R. A. Schiffer, 1999: Advances in Understanding Clouds from ISCCP. *Bull. Amer. Meteor. Soc*., **80**, 2261-2287.

Ruane, A. C., and J. O. Roads, 2007a: The Diurnal Cycle of Water and Energy over the Continental United States from Three Reanalyses. *J. Meteor. Soc. Japan,* **85A**, 117-143.

Ruane, A. C., and J. O. Roads, 2007b: 6-Hour to 1-Year Variance of Five Global Precipitation Sets. *Earth Interactions,* **11**, doi:10.1175/EI225.1.

Ruane, A. C. and J. O. Roads, 2008a: Dominant balances and exchanges of the atmospheric water cycle in the reanalysis at diurnal, annual, and intraseasonal time scales. *J. Climate*. in press.

Ruane, A. C. and J. O. Roads, 2008b: Diurnal to annual precipitation sensitivity to convective and land surface schemes. *Earth Interactions*, in review.

Schlosser, C. A., and P. R. Houser, 2007: Assessing a Satellite-Era Perspective of the Global Water Cycle, *J. Climate*, **20**, 1316-1338.

Schubert, S. D., R. B. Rood, and J. Pfaendtner, 1993: An Assimilated Dataset for Earth Science Applications. *Bull. Amer. Meteor. Soc*., **77**, 437-471.

Stackhouse, P. W., S. K. Gupta, S. J. Cox, M. Chiacchio, and J. C. Mikovitz, 2000: The WCRP/GEWEX Surface Radiation Budget Project Release 2: An assessment of surface

fluxes at 1 degree resolution. In IRS 2000: *Current Problems in Atmospheric Radiation*, W. L. Smith and Y. M. Timofeyev, Eds., International Radiation Symposium, St. Petersburg, Russia, July 24-29, 2000.

Staylor, W. F., 1985: Reflection and Emission Models for Clouds Derived from Nimbus 7 Earth Radiation Budget Scanner Measurements. *J. Geophys. Res.*, **90**, 8075-8079.

Szeto, K. K., H. Tran, M. D. MacKay, R. Crawford, and R. E. Stewart, 2008: The MAGS Water and Energy Budget Study. *J. Hydrometeor*., **9**, 96-115.

Trenberth, K. E., and C. J. Guillemot, 1998: Evaluation of the atmospheric moisture and hydrological cycle in the NCEP/NCAR reanalyses. *Climate Dyn*., **14**, 213-231.

Trenberth, K. E., J. M. Caron, and D. P. Stepaniak, 2001: The atmospheric energy budget and implications for surface fluxes and ocean heat transports. *Climate Dyn*., **17**, 259-276.

Trenberth, K. E., D. P. Stepaniak and J. M. Caron, 2002: Accuracy of atmospheric energy budgets. *J. Climate*, **15**, 3343-3360.

Trenberth, K. E., and D. P. Stepaniak, 2003a: Co-variability of components of poleward atmospheric energy transports on seasonal and interannual timescales. *J. Climate*, **16**, 3691-3705.

Trenberth, K. E., and D. P. Stepaniak, 2003b: Seamless poleward atmospheric energy transports and implications for the Hadley circulation. *J. Climate*, **16**, 3706-3722.

Trenberth, K. E., J. Fasullo, and L. Smith, 2005: Trends and variability in column-integrated atmospheric water vapor. *Climate Dyn.*, **24**(7-8), 741-758.

Trenberth, K. E., L. Smith, T. Qian, A. Dai and J. Fasullo, 2007a: Estimates of the global water budget and its annual cycle using observational and model data. *J. Hydrometeor*., **8**, 758-769.

Trenberth, K. E., and Coauthors, 2007b: Observations: Surface and Atmospheric Climate Change. In: Climate Change 2007. The Physical Science Basis. Contribution of WG 1 to the Fourth Assessment Report of the Intergovernmental Panel on Climate Change. [S. Solomon, D. Qin, M. Manning, Z. Chen, M. C. Marquis, K. B. Averyt, M. Tignor and H. L. Miller (eds)]. Cambridge University Press. Cambridge, U. K., and New York, NY, USA, 235-336, plus annex online.

Uppala, S. M., and Coauthors, 2005: The ERA-40 re-analysis. *Q. J. R. Meteorol. Soc*., **131**, 2961-3012. doi:10.1256/qj.04.176.

Viterbo, P., A. Beljaars, J. –F. Mahfouf, and J. Teixeira, 1999: The representation of soil moisture freezing and its impact on the stable boundary layer. *Q. J. R. Meteorol. Soc*., **125**, 2401–2426.

Xie, P. and P. A. Arkin, 1997: Global precipitation: A 17-year monthly analysis based on gauge observations, satellite estimates, and numerical model outputs. *Bull. Amer. Meteor. Soc*., **78**, 2539-2558.

Yang, D. Q., D. Kane, Z. P. Zhang, D. Legates, and B. Goodison, 2005: Bias corrections of long-term (1973-2004) daily precipitation data over the northern regions. *Geophys. Res. Lett*., **32**, L19501, doi:10.1029/2005GL024057.

Yin, X. G., A. Gruber, and P. Arkin, 2004: Comparison of the GPCP and CMAP merged gauge-satellite monthly precipitation products for the period 1979-2001. *J. Hydrometeor*., **5**, 1207-1222.

Yu, R. C., M. H. Zhang, and R. D. Cess, 1999: Analysis of the atmospheric energy budget: A consistency study of available data sets. *J. Geophys. Res*., **104**, 9655-9661.

Zhang, Y. -C., W. B. Rossow, and A. A. Lacis, 1995: Calculation of surface and top of atmosphere radiative fluxes from physical quantities based on ISCCP data sets: 1. Method and sensitivity to input data uncertainties, *J. Geophys. Res*., **100**, 1149 – 1165.

Zhang, Y. -C., W. B. Rossow, A. A. Lacis, V. Oinas and M. I. Mishchenko, 2004: Calculation of radiative fluxes from the surface to top-of-atmosphere based on ISCCP and other global datasets: Refinements of the radiative transfer model and the input data. *J. Geophys. Res*., **109**, doi 10.1029/2003JD004457

Table and Figure Legends

Table 1. WEBS (1986-1995) variables, which are defined in the text. Their global availability is indicated by x = global; o = ocean only; y = land only; z = computed. Rmean=(R1+R2+ERA40+JRA25)/4. Gmean = (CLM+MOS+Noah)/3. Est1 = first observational estimate. Est2 = 2nd observational estimate. The observational estimates, reanalysis models, and GLDAS models are described in the text. Est = (Est1+dEst2)/e, where e=1 if d=0 and e=2 if d=1. Total ocean N is known from conservation of mass.

Table 2 1986-1995 Annual means of the WEBS variables observational estimate.

Table 3. 1986-1995 Annual standard deviations of the WEBS variables observational estimate.

Table 4. 1986-1995 "Average" spatial RMS errors for the combined WEBS variables observational estimates and model estimates.

Fig. 1 Annual mean precipitation from two observation estimates, 3 of the 4 reanalysis models (R1, ERA40, JRA25), the Reanalysis mean (Rmean), the GLDAS mean (Gmean), and the mean of Rmean and Gmean. The areas outlined in white correspond to the RHPs described in the text.

Fig. 2 Monthly mean precipitation from two observation estimates, shown by the dark squares, 4 reanalysis models, shown by the colored circles, and 3 GLDAS model simulations, shown by the colored squares. Also shown are the Reanalysis mean (Rmean) - the large yellow circle and the

GLDAS mean (Gmean) - the large yellow square. The continuous lines denote the estimated observational mean plus or minus one 10-year standard deviation.

F**ig. 3a** Annual mean 2 m temperature for each of the identified regions. The two observational estimates are shown by the black and gray squares. These observational estimates straddle their mean plus or minus one standard deviation of 10-year means, shown by the hatched lines. Individual reanalyses are shown by the small circles and their mean is shown by the large yellow circle. Individual GLDAS simulations are shown by the small squares and their mean is shown by the large yellow square. F**ig. 3b** Annual mean precipitable water. **Fig. 3c** Annual mean T2m-Ts. F**ig. 3d** Annual mean soil moisture.

F**ig. 4a** Annual mean precipitation for each of the diagnosed regions. The two observational estimates are shown by the black and gray squares. These observational estimates straddle their mean plus or minus one standard deviation of 10-year means, shown by the hatched lines. Individual reanalyses are shown by the small circles and their mean is shown by the large yellow circle. Individual GLDAS simulations are shown by the small squares and their mean is shown by the large yellow square. F**ig. 4b** Annual mean moisture convergence. F**ig. 4c** Annual mean evaporation. **Fig. 4d** Annual mean runoff.

F**ig. 5a** Annual mean net radiation flux at the top of the atmosphere, NR-0. The two observational estimates are shown by the black and gray squares. These observational estimates straddle their mean plus or minus one standard deviation of 10-year means, shown by the hatched lines. Individual reanalyses are shown by the small circles and their mean is shown by

the large yellow circle. Individual GLDAS simulations are shown by the small squares and their mean is shown by the large yellow square. F**ig. 5b** Annual mean net radiative flux (negative) at the bottom of the atmosphere, QRS. F**ig. 5c** Annual mean transport of sensible and latent energy, EC+LMC. **Fig. 5d** Annual mean surface sensible heating plus latent heating, SH+LE.

Fig. 6a Global annual mean water budget terms, including precipitation, P, evaporation, E, moisture convergence, MC, runoff, N, and the two closure errors for the surface water, EW, and the atmospheric water vapor, EQ. There are two observation estimates, shown by the dark squares, 4 reanalysis models, shown by the colored circles, and 3 GLDAS model simulations, shown by the colored squares. Also shown are the Reanalysis mean (Rmean) - the large yellow circle and the GLDAS mean (Gmean) - the large yellow square. The horizontal lines in the observational estimate columns denote the observational estimated mean plus or minus 1 standard deviation for 10-year means for that variable. **Fig. 6b** Global annual mean energy budget terms, including the negative of the atmospheric net radiative cooling, QR, latent heat released by precipitation, LP, dry static energy convergence, EC, sensible heating, SH, latent heating, LE, surface radiative, QRS, and the two combination closure, tendency or closure error terms for the surface energy, EG, and the atmospheric energy, ET.

Fig. 7a Ocean annual mean water budget terms, including precipitation, P, evaporation, E, moisture convergence, MC, runoff, N, and the closure error for the surface water, EW and EQ. There are two observation estimates, shown by the dark squares, 4 reanalysis models, shown by the colored circles. Also shown are the HOAPS-3 and GSSTF2 means. The horizontal lines in the observational estimate columns denote the observational estimated mean plus or minus 1

standard deviation for 10-year means for that variable. **Fig. 7b** Ocean annual mean energy budget terms, including the negative of the atmospheric net radiative cooling, QR, latent heat released by precipitation, LP, dry static energy convergence, EC, sensible heating, SH, latent heating, LE, surface radiative, QRS, and the two combination closure, tendency error terms for the surface energy, EG, and the atmospheric energy, ET.

Fig. 8a Terrestrial annual mean water budget terms, including precipitation, P, evaporation, E, moisture convergence, MC, runoff, N, and the two combination closure and negative tendency error terms for the surface water, EW, and the atmospheric water vapor, EQ. There are two observation estimates, shown by the dark squares, 4 reanalysis models, shown by the colored circles, and 3 GLDAS model simulations, shown by the colored squares. Also shown are the Reanalysis mean (Rmean) - the large yellow circle and the GLDAS mean (Gmean) - the large yellow square. The horizontal lines in the observational estimate columns denote the observational estimated mean plus or minus 1 standard deviation for 10-year means for that variable. **Fig. 8b** Terrestrial annual mean energy budget terms, including the negative of the atmospheric net radiative cooling, QR, latent heat released by precipitation, LP, dry static energy convergence, EC, sensible heating, SH, latent heating, LE, surface radiative, QRS, and the two combination closure, tendency error terms for the surface energy, EG, and the atmospheric dry static energy, ET.

Fig. 9a Closure errors in the annual mean surface energy budget from two observation estimates, shown by the dark squares in comparison to 4 reanalysis models, shown by the colored circles, and 3 GLDAS model simulations, shown by the colored squares. Also shown are the Reanalysis

mean (Rmean) - the large yellow circle and the GLDAS mean (Gmean) - the large square. The horizontal lines in the observation estimates denote the estimated observation mean plus or minus 1 standard deviation for 10-year means. **Fig. 9b** Closure error in the annual mean surface water budget. **Fig. 9c** Closure error in the annual mean atmospheric energy budget. **Fig. 9d** Closure error in the annual mean atmospheric water budget.

Fig. 10a Spatial RMS of precipitation from two observation estimates, shown by the dark squares in comparison to 4 reanalysis models, shown by the colored circles, and 3 GLDAS model simulations, shown by the colored squares. Also shown are the Reanalysis mean (Rmean) - the large yellow circle and the GLDAS mean (Gmean) - the large square. The horizontal lines in the observation estimates denote the estimated observation mean plus or minus 1 standard deviation for 10-year means. **Fig. 10b** Spatial RMS of moisture convergence. **Fig. 10c** Spatial RMS evaporation. **Fig. 10d** Spatial RMS of runoff.

F**ig. 11a** Spatial RMS of net radiation flux at the top of the atmosphere, NR-0. The two observational estimates are shown by the black and gray squares. These observational estimates straddle their mean plus or minus one standard deviation of 10-year means, shown by the hatched lines. Individual reanalyses are shown by the small circles and their mean is shown by the large yellow circle. Individual GLDAS simulations are shown by the small squares and their mean is shown by the large yellow square. F**ig. 11b** Spatial RMS of net radiative flux (negative) at the bottom of the atmosphere, QRS. F**ig. 11c** Spatial RMS of transport of sensible and latent energy, EC+LMC. **Fig. 11d** Spatial RMS of surface sensible heating plus latent heating, SH+LE

Table 1. WEBS (1986-1995) variables, which are defined in the text. Their global availability is indicated by x = global; o = ocean only; y = land only; z = computed. Rmean=(R1+R2+ERA40+JRA25)/4. Gmean = (CLM+MOS+Noah)/3. Est1 = first observational estimate. Est2 = 2nd observational estimate. The observational estimates, reanalysis models, and GLDAS models are described in the text. Est = (Est1+dEst2)/e, where e=1 if d=0 and e=2 if d=1. Total ocean N is known from conservation of mass.

	Variable	units	Est1	Est2	R1	R2	ERA40	JRA25	CLM	Noah	MOS
1.	**P**	mm/day	GPCP	CMAP	x	x	x	x	y	y	y
2.	**E**	mm/day	HOAPSo+RMEANy	GSSTF2o+GMEANy	x	x	x	x	y	y	y
3.	**N**	mm/day	ISLSCP	GRDC	x	x	x	x	x	x	x
4.	**MC**	mm/day	RI	ERA40	z	z	z	z			
5.	**Snow**	mm	Rmean	Gmean	y	y	y	y	y	y	y
6.	**Soilm**	mm	Rmean	Gmean	y	y	y	y	y	y	y
7.	**Q**	mm	NVAP	ISCCP FD	x	x	x	x			
8.	**Ts**	K	Rmean	Gmean	x	x	x	x	y	y	y
9.	**T2m**	K	CRU	CPC	x	x	x	x	y	y	y
10.	**T2m-Ts**	K	Rmean	Gmean	x	x	x	x	y	y	y
11.	**CpT**	J/m^2	ERA40	RII							
12.	**LP**	W/m^2	GPCP	CMAP	z	z	z	z			
13.	**EC**	W/m^2	R1	ERA40	z	z	z	z			
14.	**SH**	W/m^2	HOAPSo+RMEANy	GSSTF2o+GMEANy	x	x	x	x	y	y	y
15.	**LE**	W/m^2	HOAPSo+RMEANy	GSSTF2o+GMEANy	x	x	x	x	y	y	y
16.	**EQ**	mm/day	z	z	z	z	z	z			
17.	**EW**	mm/day	z	z	z	z	z	z	z	z	z
18.	**DSW-1**	W/m^2	SRB	ISCCP FD	x	x	x	x	y	y	y
19.	**DLW-1**	W/m^2	SRB	ISCCP FD	x	x	x	x	y	y	y
20.	**USW-1**	W/m^2	SRB	ISCCP FD	x	x	x	x	y	y	y
21.	**ULW-1**	W/m^2	SRB	ISCCP FD	x	x	x	x	y	y	y
22.	**DSW-0**	W/m^2	SRB	ISCCP FD	x	x	x	x			
23.	**USW-0**	W/m^2		ISCCP FD	x	x	x	x			
24.	**ULW-0**	W/m^2	SRB	ISCCP FD	x	x	x	x			
25.	**NSW-1**	W/m^2	SRB	ISCCP FD	x	x	x	x	y	y	y
26.	**NLW-1**	W/m^2	SRB	ISCCP FD	x	x	x	x	y	y	y
27.	**NSW-0**	W/m^2	SRB	ISCCP FD	x	x	x	x			
28.	**QR**	W/m^2	SRB	ISCCP FD	x	x	x	x			
29.	**QRS**	W/m^2	SRB	ISCCP FD	x	x	x	x	y	y	y
30.	**LE+SH**	W/m^2	HOAPSo+RMEANy	GSSTF2o+GMEANy	z	z	z	z	z	z	z
31.	**NR-0**	W/m^2	SRB	ISCCP FD	z	z	z	z	z	z	z
32.	**EC+LMC**	W/m^2	R1	ERA40	z	z	z	z			
33.	**ET**	W/m^2	z	z	z	z	z	z			
34.	**EG**	W/m^2	z	z	z	z	z	z	z	z	z

Table 2: 1986-1995 Estimated Annual Means of the WEBS variables observational estimate

	units	Var	Lena	MAGS	Tibet	BALTEX	GAPP	HUBEX	MDB	LPB	LBA	Game-T	AMMA	Land	Ocean	Global
	km^2	**AREA**	2.12e6	1.50e6	2.95e6	1.56e6	8.13e6	3.70e5	1.35e6	3.74e6	5.99e6	2.71e6	2.96e6	1.45e8	3.51e8	5.11e8
1.	mm/dy	**P**	1.03	1.07	1.15	1.89	1.97	2.68	1.72	3.42	5.16	5.30	2.12	2.13	2.92	2.63
2.	mm/dy	**E**	0.93	1.08	1.08	1.29	1.80	2.11	1.55	2.83	3.49	3.58	1.56	1.68	3.27	2.73
3.	mm/dy	**N**	0.38	0.32	0.79	0.70	0.62	0.42	0.12	0.81	3.10	2.95	0.63	0.88	0.46	0.00
4.	mm/dy	**MC**	0.49	0.57	1.27	0.66	0.52	-0.08	-0.09	0.21	1.64	2.30	0.79	0.64	-0.29	0.00
5.	mm	**Snow**	43.3	36.4	4.56	25.4	3.78	0.08	0.00	0.01	0.01	0.00	0.00	177	NA	NA
6.	mm	**Soilm**	488	452	436	564	400	453	297	432	535	522	311	417	NA	NA
7.	mm	**Q**	8.20	9.50	10.3	13.4	17.0	24.4	19.7	27.5	40.7	43.9	31.4	22.1	27.5	25.4
8.	K	**Ts**	264	270	275	277	284	288	291	293	297	298	301	286	291	288
9.	K	**T2m**	265	271	278	278	285	288	291	294	298	300	301	287	291	288
10.	K	**T2m-Ts**	0.89	0.58	-0.80	1.18	-0.03	-0.07	-0.23	0.25	0.46	0.18	-1.06	-0.12	-0.73	-0.54
11.	J/m^2	**CpT**	2.34e9	2.33e9	1.57e9	2.50e9	2.38e9	2.59e9	2.56e9	2.51e9	2.52e9	2.57e9	2.53e9	2.43e9	2.61e9	2.54e9
12.	W/m^2	**LP**	29.9	31.0	33.3	54.7	57.0	77.7	49.9	99.0	149	153	61.2	61.5	84.5	76.2
13.	W/m^2	**EC**	40.1	20.9	-45.2	10.1	13.2	31.5	43.4	-45.1	-100	-118	-40.2	-3.66	-1.00	0.92
14.	W/m^2	**SH**	7.71	7.96	37.4	-5.83	32.2	27.5	54.1	29.1	25.2	23.0	63.6	34.9	11.1	16.7
15.	W/m^2	**LE**	26.4	31.1	31.2	36.9	52.0	60.9	44.8	81.7	101	103	44.9	48.3	93.7	78.4
16.	mm/dy	**EQ**	-0.38	-0.58	-1.20	-0.06	-0.36	0.65	0.26	0.38	0.04	-0.58	-0.23	-0.20	-0.06	-0.10
17.	mm/dy	**EW**	0.27	0.34	0.71	0.10	0.45	-0.15	-0.05	0.22	1.42	1.23	0.07	0.43	-0.12	0.10
18.	W/m^2	**DSW-1**	119	122	195	111	179	168	209	206	205	216	246	188	191	188
19.	W/m^2	**DLW-1**	240	261	254	289	316	340	333	363	397	408	394	331	358	344
20.	W/m^2	**USW-1**	26.7	23.6	39.8	19.1	25.4	20.2	25.2	27.5	26.9	22.0	57.3	34.3	14.9	22.5
21.	W/m^2	**ULW-1**	281	303	320	331	376	392	411	422	429	445	465	387	404	393
22.	W/m^2	**DSW-0**	234	238	355	244	332	357	357	378	411	407	405	340	347	340
23.	W/m^2	**USW-0**	91.1	89.2	130	97.5	107	125	96.6	114	135	118	119	110	99.7	103
24.	W/m^2	**ULW-0**	198	207	213	216	229	229	250	242	229	233	260	234	236	233
25.	W/m^2	**NSW-1**	-91.9	-98.0	-155	-91.5	-154	-148	-184	-179	-178	-194	-189	-153	-176	-165
26.	W/m^2	**NLW-1**	40.7	41.8	65.1	41.9	59.3	51.7	78.8	59.3	31.7	36.6	70.5	55.9	46.4	48.5
27.	W/m^2	**NSW-0**	-143	-148	-225	-147	-225	-232	-260	-264	-276	-288	-286	-230	-247	-237
28.	W/m^2	**QR**	-107	-115	-77.8	-119	-97.8	-93.5	-94.5	-98.1	-99.1	-102	-92.2	-101	-119	-113
29.	W/m^2	**QRS**	51.2	56.2	90.0	49.6	94.3	95.8	105	120	146	157	118	97.5	130	117
30.	W/m^2	**LE+SH**	34.1	39.1	68.5	31.0	84.2	88.4	98.9	111	126	129	109	83.1	105	95.0

31.	W/m^2	**NR-0**	55.8	58.9	-12.2	69.4	3.45	-2.32	-10.6	-21.6	-47.3	-55.2	-26.2	3.56	-11.0	-3.84
32.	W/m^2	**EC+LMC**	54.2	37.3	-8.40	29.2	28.3	29.2	40.6	-39.0	-52.5	-51.0	-17.4	15.0	-9.30	0.90
33.	W/m^2	**ET**	29.4	55.2	52.4	60.1	-4.54	-43.1	-52.8	15.1	24.5	43.4	7.50	8.34	23.8	19.2
34.	W/m^2	**EG**	-17.2	-17.1	-21.4	-18.6	-10.1	-7.42	-6.23	-8.87	-20.6	-31.3	-9.85	-14.3	-24.7	-21.8

Table 3: 1986-1995 Annual standard deviations of the WEBS variables observational estimate

	units	Var	Lena	MAGS	Tibet	BALTEX	GAPP	HUBEX	MDB	LPB	LBA	Game-T	AMMA	Land (90N-60S)	Ocean	Global
1.	mm/dy	**P**	.099	0.11	.077	.049	0.13	0.41	0.26	0.24	0.25	0.34	0.18	.054	.026	.025
2.	mm/dy	**E**	.038	.049	.017	.054	.057	.069	0.16	0.11	.092	.037	.043	.023	.117	.078
3.	mm/dy	**N**	.053	.039	.086	.035	.064	0.21	.047	.092	0.26	0.29	.072	.033	.018	NA
4.	mm/dy	**MC**	0.12	.091	0.15	.094	0.11	0.37	0.18	0.18	0.25	0.25	0.11	.032	.015	1.5e-3
5.	mm	**Snow**	2.96	4.18	0.49	4.01	0.72	0.047	4.3e-4	1.5e-3	5.3e-4	0.00	0.00	2.34	NA	NA
6.	mm	**Soilm**	11.4	5.86	2.58	9.77	12.0	16.6	15.8	10.4	18.3	12.2	5.21	3.30	NA	NA
7.	mm	**Q**	0.36	0.36	0.48	0.63	0.49	0.68	0.58	0.80	1.47	1.36	1.41	0.57	0.39	0.38
8.	K	**Ts**	0.91	0.65	0.27	0.90	0.32	0.26	0.46	0.27	0.22	0.15	0.32	0.14	.063	.088
9.	K	**T2m**	0.92	0.69	0.28	0.86	0.37	0.31	0.31	0.27	0.15	0.13	0.33	0.17	0.13	.089
10.	K	**T2m-Ts**	0.12	.093	0.13	.058	.050	0.15	0.17	.090	.070	.064	0.15	.045	.033	.024
11.	J/m^2	**CpT**	7.1e3	4.1e3	4.5e3	5.0e3	6.1e3	5.3e3	4.0e3	9.2e2	2.4e2	4.4e2	2.6e2	2.7e3	3.7e2	2.3e2
12.	W/m^2	**LP**	1.78	1.68	2.15	2.68	4.09	3.33	5.48	5.96	6.96	8.82	3.86	0.92	0.75	0.47
13.	W/m^2	**EC**	7.50	5.98	8.96	7.32	4.88	24.2	13.3	7.57	13.8	8.81	7.19	2.19	0.99	0.16
14.	W/m^2	**SH**	1.81	2.36	1.65	0.95	1.92	2.80	3.83	2.62	3.41	1.50	1.85	1.06	0.54	0.62
15.	W/m^2	**LE**	1.10	1.47	0.51	1.62	1.64	2.00	4.65	3.05	2.65	1.08	1.24	0.68	3.57	2.40
16.	mm/dy	**EQ**	.061	.090	0.13	.069	.084	0.15	0.14	0.20	0.35	0.24	.098	.043	0.11	0.07
17.	mm/dy	**EW**	.060	.072	.057	.060	.088	0.20	0.14	0.12	0.18	0.18	.089	.028	0.12	0.07
18.	W/m^2	**DSW-1**	3.08	1.91	2.19	3.27	2.42	5.36	3.80	3.76	3.56	3.10	2.62	0.91	1.51	1.26
19.	W/m^2	**DLW-1**	3.98	1.89	2.65	3.96	1.54	3.17	3.35	1.89	1.98	2.24	3.78	1.33	1.37	1.30
20.	W/m^2	**USW-1**	1.76	1.45	2.61	2.34	1.94	1.37	1.61	3.01	4.47	1.43	4.10	1.21	0.21	0.45
21.	W/m^2	**ULW-1**	3.98	2.73	1.85	4.01	1.98	2.15	2.59	2.69	2.22	2.44	3.81	1.28	1.44	1.29
22.	W/m^2	**DSW-0**	0.22	0.22	.092	0.16	0.11	.090	.085	.070	.020	.046	.053	.047	.059	.063
23.	W/m^2	**USW-0**	2.40	1.95	1.94	2.91	3.59	4.41	3.95	5.26	4.90	3.33	4.01	1.37	1.57	1.41
24.	W/m^2	**ULW-0**	1.53	1.45	1.26	1.68	1.65	1.86	2.66	2.79	2.72	2.36	2.84	0.83	0.60	0.64
25.	W/m^2	**NSW-1**	2.78	2.22	2.14	3.44	3.92	4.70	4.21	6.01	5.88	3.58	4.57	1.57	1.65	1.51
26.	W/m^2	**NLW-1**	1.92	1.63	3.10	1.15	1.69	3.23	4.14	2.14	1.51	3.86	2.86	1.06	1.52	1.33
27.	W/m^2	**NSW-0**	2.42	2.05	1.96	2.86	3.60	4.39	3.89	5.27	4.91	3.35	4.02	1.40	1.56	1.40
28.	W/m^2	**QR**	1.73	1.31	2.27	1.84	1.14	3.05	2.71	2.27	3.19	2.67	2.61	1.34	1.71	1.53
29.	W/m^2	**QRS**	1.65	2.19	3.44	2.91	2.60	2.74	2.34	4.99	5.79	3.92	4.00	1.65	1.27	1.30
30.	W/m^2	**LE+SH**	1.24	1.52	1.88	0.94	1.20	2.26	1.36	1.53	2.48	1.49	1.63	0.74	3.85	2.76
31.	W/m^2	**NR-0**	1.86	1.75	1.85	2.74	2.46	3.87	2.13	4.38	5.06	3.45	4.81	1.16	1.52	1.34

32.	W/m^2	**EC+LMC**	6.03	5.37	5.87	6.39	3.60	17.6	10.9	5.93	7.91	5.64	6.55	2.18	0.95	0.15
33.	W/m^2	**ET**	9.51	8.88	9.90	5.40	5.06	26.9	19.1	10.8	19.9	15.4	8.46	3.94	1.80	1.58
34.	W/m^2	**EG**	1.10	2.14	3.17	2.85	3.09	3.52	3.22	5.73	7.48	4.33	4.61	2.08	4.49	3.51

Table 4: 1986-1995 “average” spatial RMS errors for all the WEBS variables, observational estimates and models

	units	Var	Lena	MAGS	Tibet	BALTEX	GAPP	HUBEX	MDB	LPB	LBA	Game-T	AMMA	Land (90N-60S)	Ocean	Global
1.	mm/dy	**P**	0.24	0.28	0.86	0.28	0.38	0.31	0.32	0.77	1.20	1.45	0.52	0.77	0.66	0.70
2.	mm/dy	**E**	0.22	0.29	0.32	0.28	0.33	0.31	0.27	0.44	0.54	0.58	0.30	0.40	0.40	0.40
3.	mm/dy	**N**	0.15	0.16	0.68	0.33	0.41	0.41	0.15	0.61	1.29	1.39	0.51	0.71	0.38	NA
4.	mm/dy	**MC**	0.38	0.45	1.24	0.53	0.60	0.65	0.52	1.08	1.42	1.55	1.01	1.10	0.66	1.06
5.	mm	**Snow**	12.8	14.0	5.25	15.5	3.76	0.09	0.00	0.04	0.05	0.00	0.00	1.29e3	NA	NA
6.	mm	**Soilm**	154	156	165	175	132	133	84.7	144	168	160	102	146	NA	NA
7.	mm	**Q**	0.45	0.53	2.95	0.52	1.16	1.08	1.65	1.81	2.53	1.98	4.90	2.64	1.65	1.98
8.	K	**Ts**	1.69	1.45	3.13	1.25	0.95	0.67	0.76	1.00	1.05	0.95	2.15	1.60	0.44	0.96
9.	K	**T2m**	1.14	1.07	5.56	0.46	1.07	0.52	0.87	1.28	1.85	1.25	1.19	1.84	1.05	1.81
10.	K	**T2m-Ts**	1.17	1.00	1.05	1.24	0.59	0.50	0.49	0.61	0.88	0.71	1.29	1.07	0.27	0.63
11.	J/m^2	**CpT**	2.40e7	2.09e7	7.64e7	21.5e7	25.1e7	24.5e7	22.3e7	19.9e7	39.0e7	32.8e7	17.7e7	40.8e7	11.3e7	34.2e7
12.	W/m^2	**LP**	7.18	8.90	26.2	8.38	11.4	10.1	7.90	22.4	36.1	43.0	16.9	23.5	19.7	21.2
13.	W/m^2	**EC**	34.7	43.9	67.2	46.6	34.7	54.7	48.0	47.3	55.5	48.5	47.6	54.5	43.7	47.7
14.	W/m^2	**SH**	11.6	13.9	15.1	9.64	14.1	4.50	9.16	11.1	17.2	12.4	20.9	16.9	6.13	10.5
15.	W/m^2	**LE**	6.03	8.47	9.33	8.15	9.56	9.01	7.71	12.6	15.5	16.7	8.44	11.6	11.7	11.6
16.	mm/dy	**EQ**	0.43	0.64	1.51	0.45	0.62	0.69	0.59	1.21	1.64	1.57	1.05	1.24	0.84	1.02
17.	mm/dy	**EW**	0.29	0.33	0.92	0.27	0.50	0.47	0.36	0.64	1.36	1.70	0.50	0.92	0.92	0.98
18.	W/m^2	**DSW-1**	12.1	12.2	32.7	15.4	18.3	21.1	16.3	21.6	24.5	18.0	19.1	20.2	11.8	15.2
19.	W/m^2	**DLW-1**	9.64	10.7	24.3	11.8	13.0	8.98	9.42	9.11	9.48	7.13	21.8	14.9	6.43	10.1
20.	W/m^2	**USW-1**	11.6	10.2	25.7	7.64	12.6	9.84	12.7	12.0	8.46	6.95	16.8	15.0	5.16	9.60
21.	W/m^2	**ULW-1**	9.57	9.16	17.0	7.90	7.68	5.07	8.17	8.64	14.0	8.24	13.4	11.1	4.97	7.74
22.	W/m^2	**DSW-0**	0.98	0.90	0.38	0.95	0.30	0.27	1.84	1.75	1.37	0.85	0.80	1.01	1.61	1.52
23.	W/m^2	**USW-0**	7.65	7.57	13.7	12.4	8.77	10.3	6.57	9.66	17.7	15.9	11.3	12.9	14.2	13.8
24.	W/m^2	**ULW-0**	5.36	5.37	10.8	6.56	10.6	8.30	9.05	14.7	19.3	10.5	11.2	10.6	9.50	9.74
25.	W/m^2	**NSW-1**	6.22	6.58	17.6	10.4	10.8	13.8	11.4	14.2	18.8	18.0	20.3	16.6	11.6	13.7
26.	W/m^2	**NLW-1**	14.6	13.4	22.1	14.4	12.7	10.4	11.7	11.3	17.9	10.7	17.5	15.5	7.70	11.4
27.	W/m^2	**NSW-0**	7.59	7.57	13.5	12.3	8.65	10.3	6.65	10.3	17.9	15.6	11.2	12.9	13.9	13.6
28.	W/m^2	**QR**	12.7	11.4	13.7	10.4	5.47	4.12	10.7	10.6	13.6	9.24	20.4	14.3	8.45	11.0
29.	W/m^2	**QRS**	13.9	12.5	19.6	11.9	9.78	9.97	9.77	11.4	24.0	24.7	21.7	18.3	12.1	15.0
30.	W/m^2	**LE+SH**	7.39	7.51	12.4	8.16	10.2	9.88	8.37	9.70	14.2	13.9	22.9	14.7	12.8	13.6
31.	W/m^2	**NR-0**	5.00	4.77	12.3	6.81	8.51	5.65	12.0	14.5	16.2	21.1	14.7	14.0	16.1	15.4

32.	W/m^2	**EC+LMC**	29.2	36.6	54.2	37.9	34.0	44.7	45.6	39.2	34.4	34.0	33.4	44.5	37.4	40.6
33.	W/m^2	**ET**	57.8	71.1	92.1	96.3	68.8	58.7	44.2	117	173	183	99.5	107	121	116
34.	W/m^2	**EG**	86.8	96.9	103	106	134	141	122	184	230	238	142	145	170	168

1986-1995 Annual Means, Precip

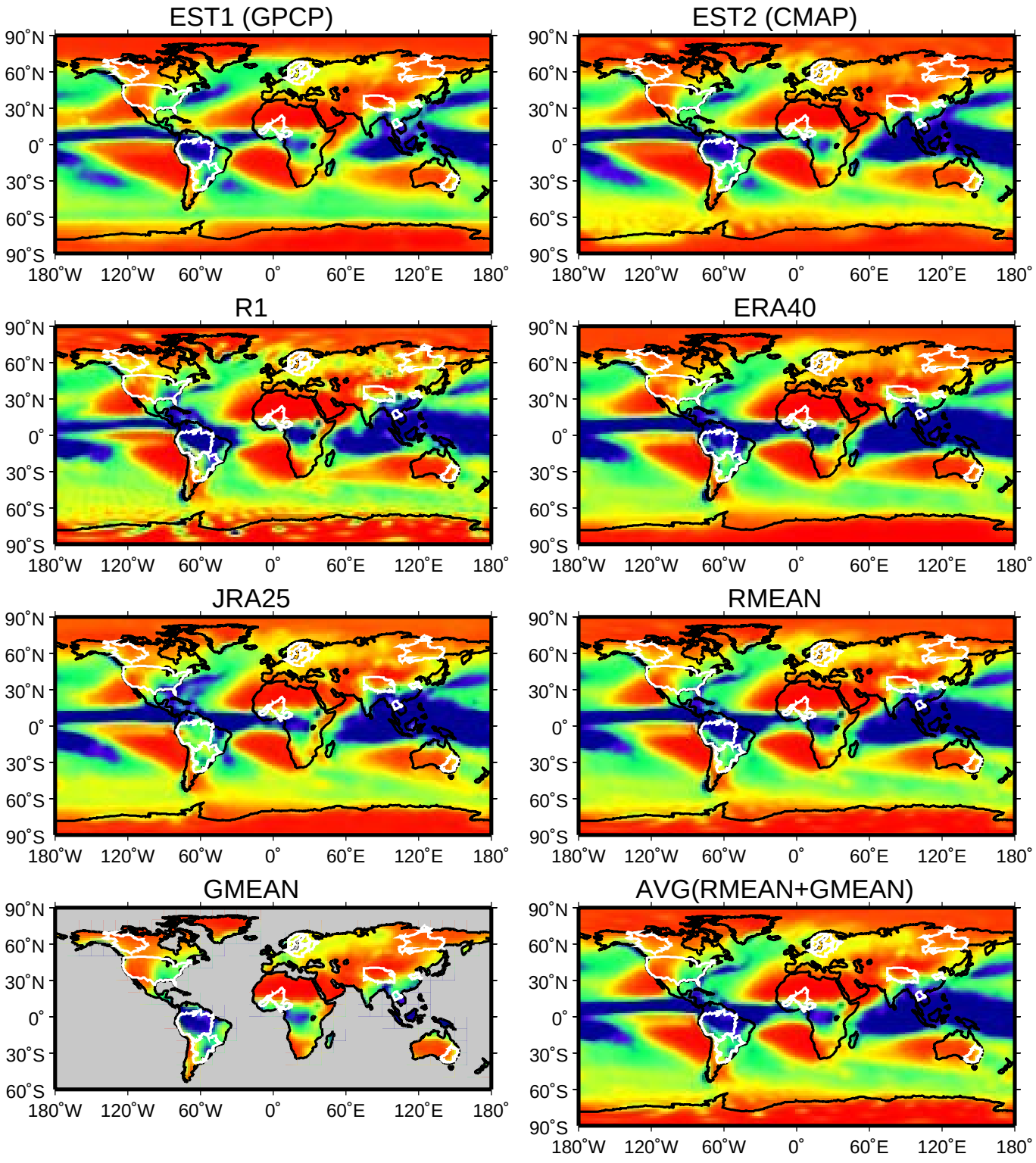

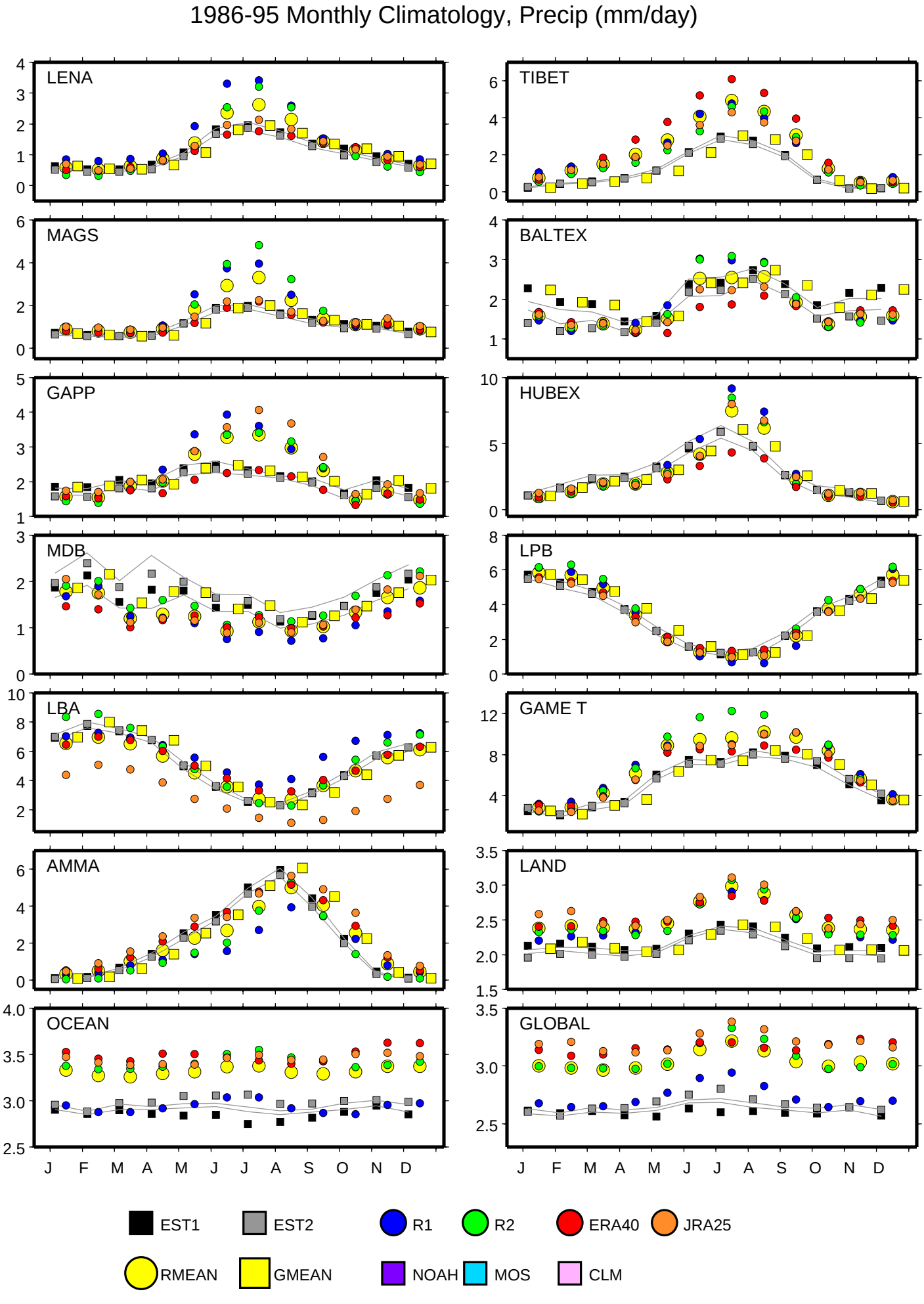
1986-95 Monthly Climatology, Precip (mm/day)
LENA
TIBET
MAGS
BALTEX
GAPP
HUBEX
MDB
LPB
LBA
GAME T
AMMA
LAND
OCEAN
GLOBAL
J F M A M J J A S O N D
EST1
EST2
R1
R2
ERA40
JRA25
RMEAN
GMEAN
NOAH
MOS
CLM

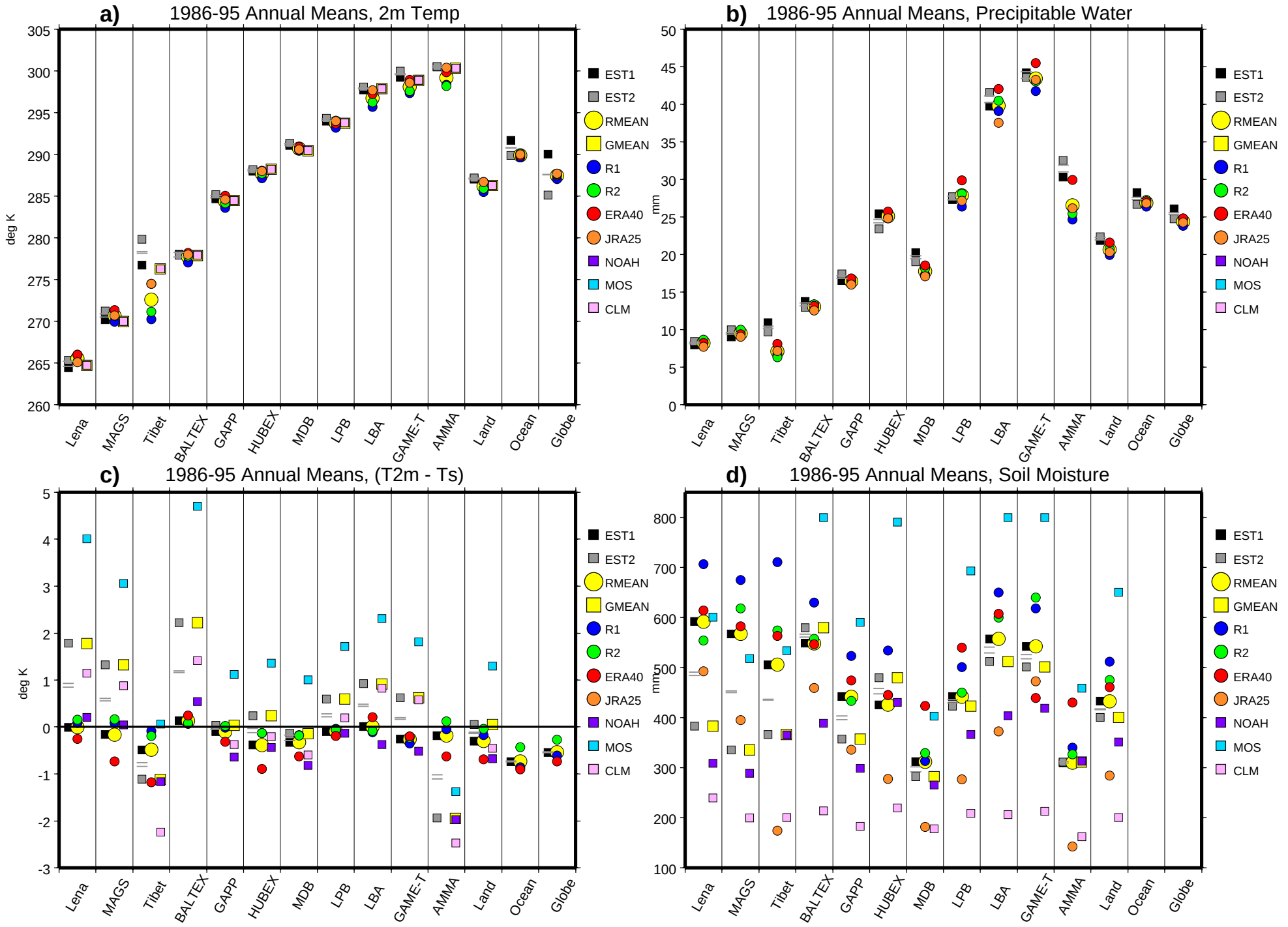
a)
1986-95 Annual Means, 2m Temp
deg K
305
300
295
290
285
280
275
270
265
260
b)
1986-95 Annual Means, Precipitable Water
mm
50
45
40
35
30
25
20
15
10
5
0
c)
1986-95 Annual Means, (T2m - Ts)
deg K
5
4
3
2
1
0
-1
-2
-3
d)
1986-95 Annual Means, Soil Moisture
mm
800
700
600
500
400
300
200
100
Lena
MAGS
Tibet
BALTEX
GAPP
HUBEX
MDB
LPB
LBA
GAME-T
AMMA
Land
Ocean
Globe
EST1
EST2
RMEAN
GMEAN
R1
R2
ERA40
JRA25
NOAH
MOS
CLM

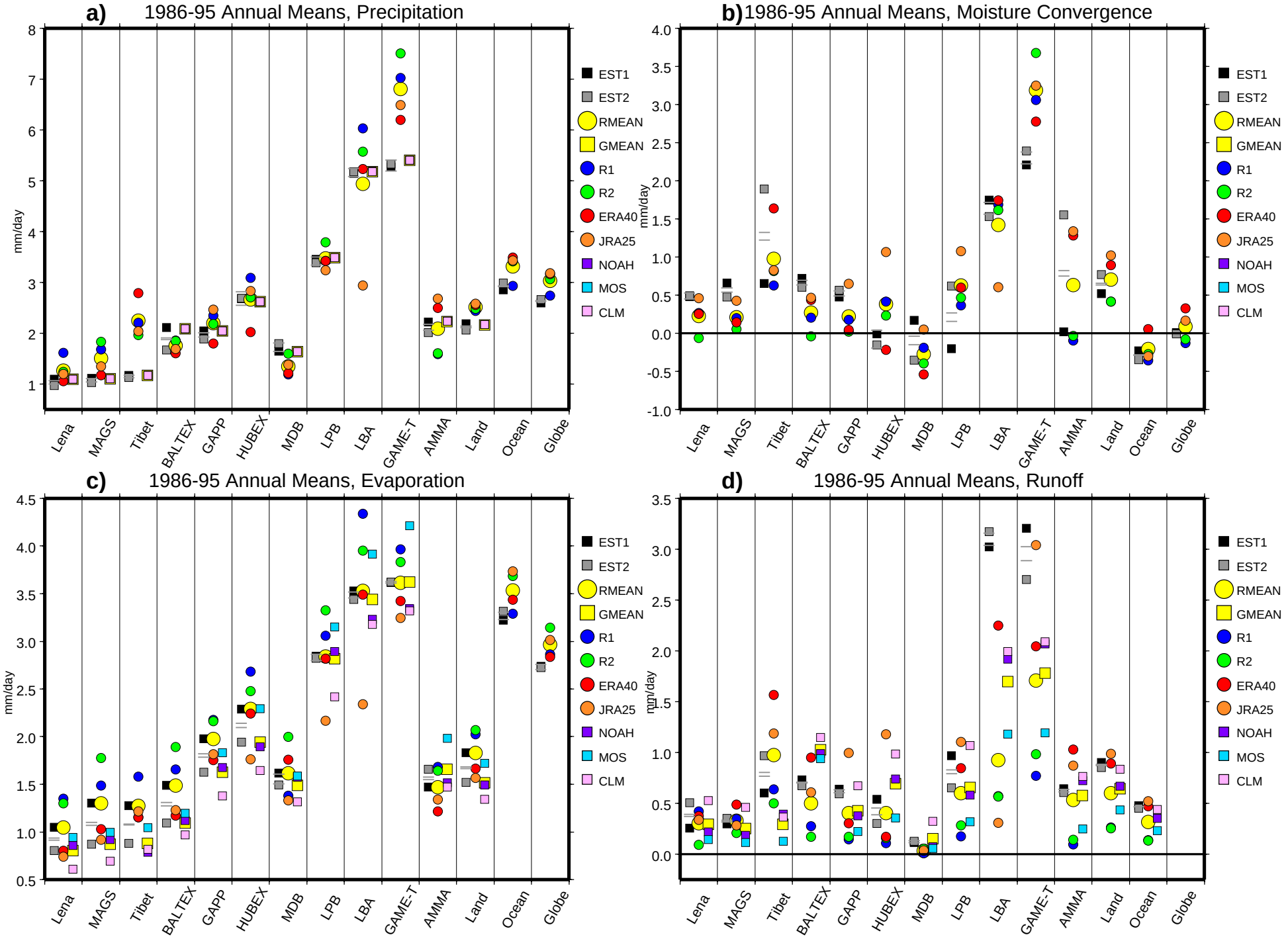
a)
1986-95 Annual Means, Precipitation
mm/day
b)
1986-95 Annual Means, Moisture Convergence
mm/day
c)
1986-95 Annual Means, Evaporation
mm/day
d)
1986-95 Annual Means, Runoff
mm/day
EST1
EST2
RMEAN
GMEAN
R1
R2
ERA40
JRA25
NOAH
MOS
CLM
Lena
MAGS
Tibet
BALTEX
GAPP
HUBEX
MDB
LPB
LBA
GAME-T
AMMA
Land
Ocean
Globe

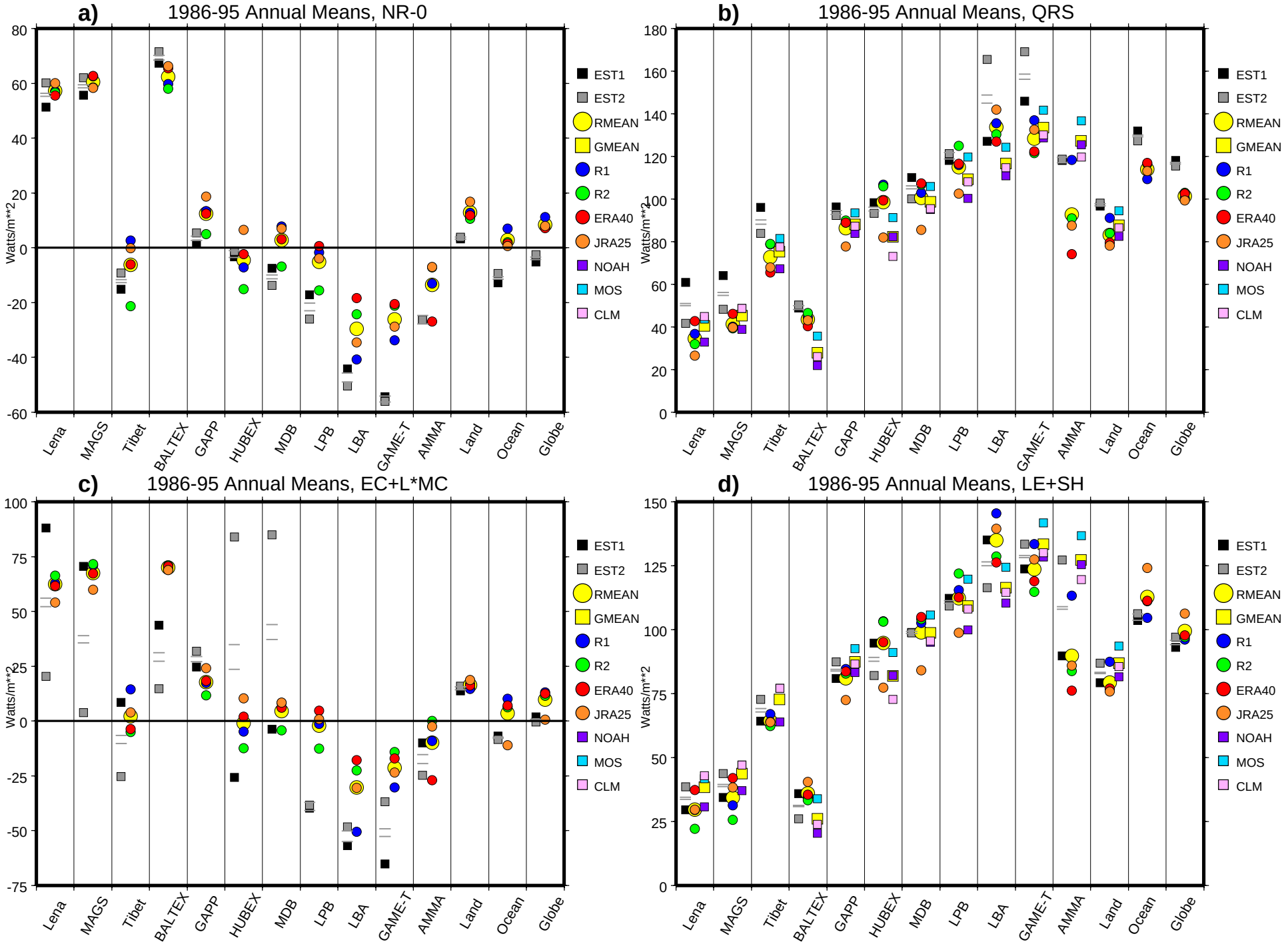
a)
1986-95 Annual Means, NR-0
b)
1986-95 Annual Means, QRS
c)
1986-95 Annual Means, EC+L*MC
d)
1986-95 Annual Means, LE+SH
Watts/m**2
EST1
EST2
RMEAN
GMEAN
R1
R2
ERA40
JRA25
NOAH
MOS
CLM
Lena
MAGS
Tibet
BALTEX
GAPP
HUBEX
MDB
LPB
LBA
GAME-T
AMMA
Land
Ocean
Globe

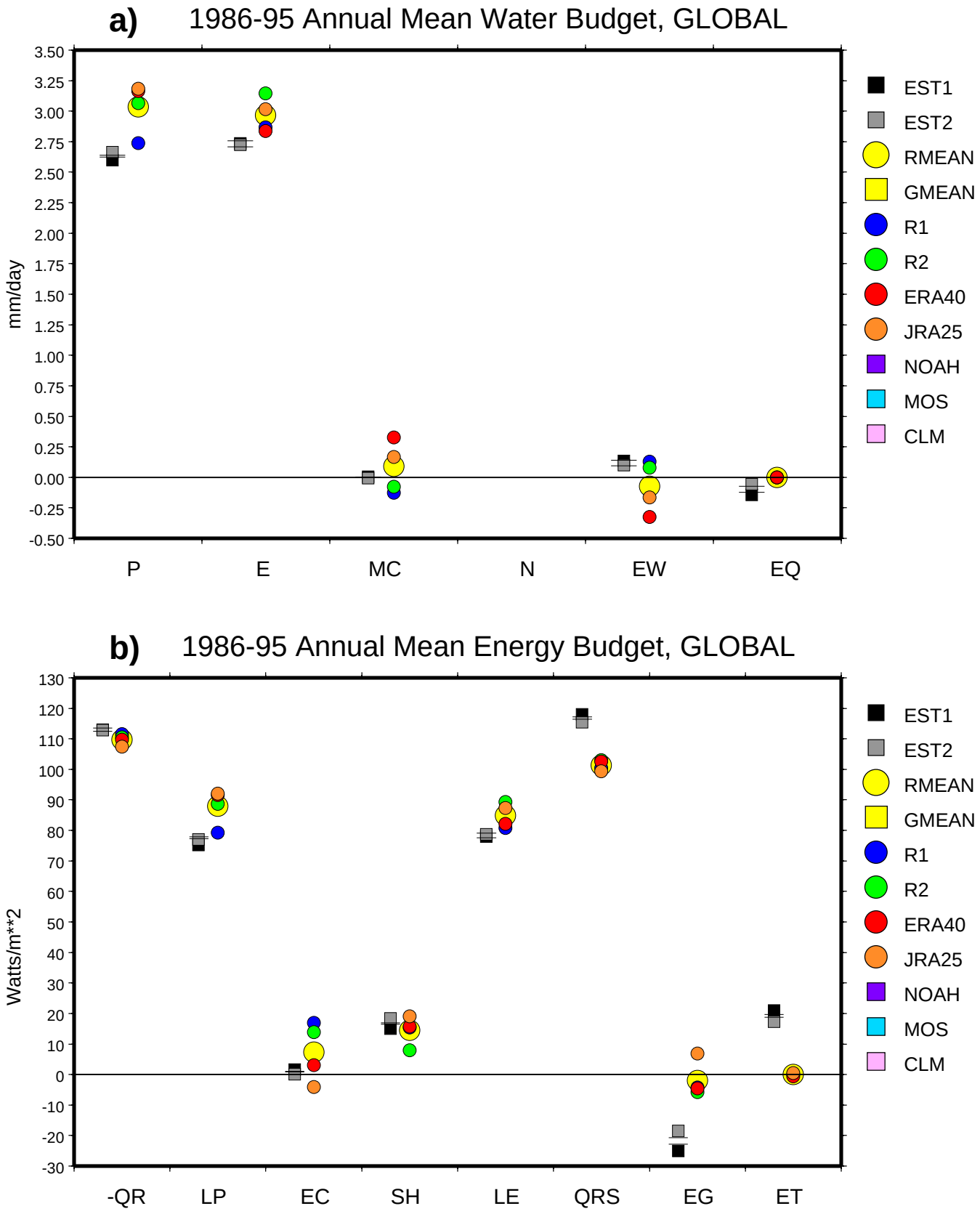
a)
1986-95 Annual Mean Water Budget, GLOBAL
mm/day
3.50
3.25
3.00
2.75
2.50
2.25
2.00
1.75
1.50
1.25
1.00
0.75
0.50
0.25
0.00
-0.25
-0.50
P
E
MC
N
EW
EQ
EST1
EST2
RMEAN
GMEAN
R1
R2
ERA40
JRA25
NOAH
MOS
CLM
b)
1986-95 Annual Mean Energy Budget, GLOBAL
Watts/m**2
130
120
110
100
90
80
70
60
50
40
30
20
10
0
-10
-20
-30
-QR
LP
EC
SH
LE
QRS
EG
ET
EST1
EST2
RMEAN
GMEAN
R1
R2
ERA40
JRA25
NOAH
MOS
CLM

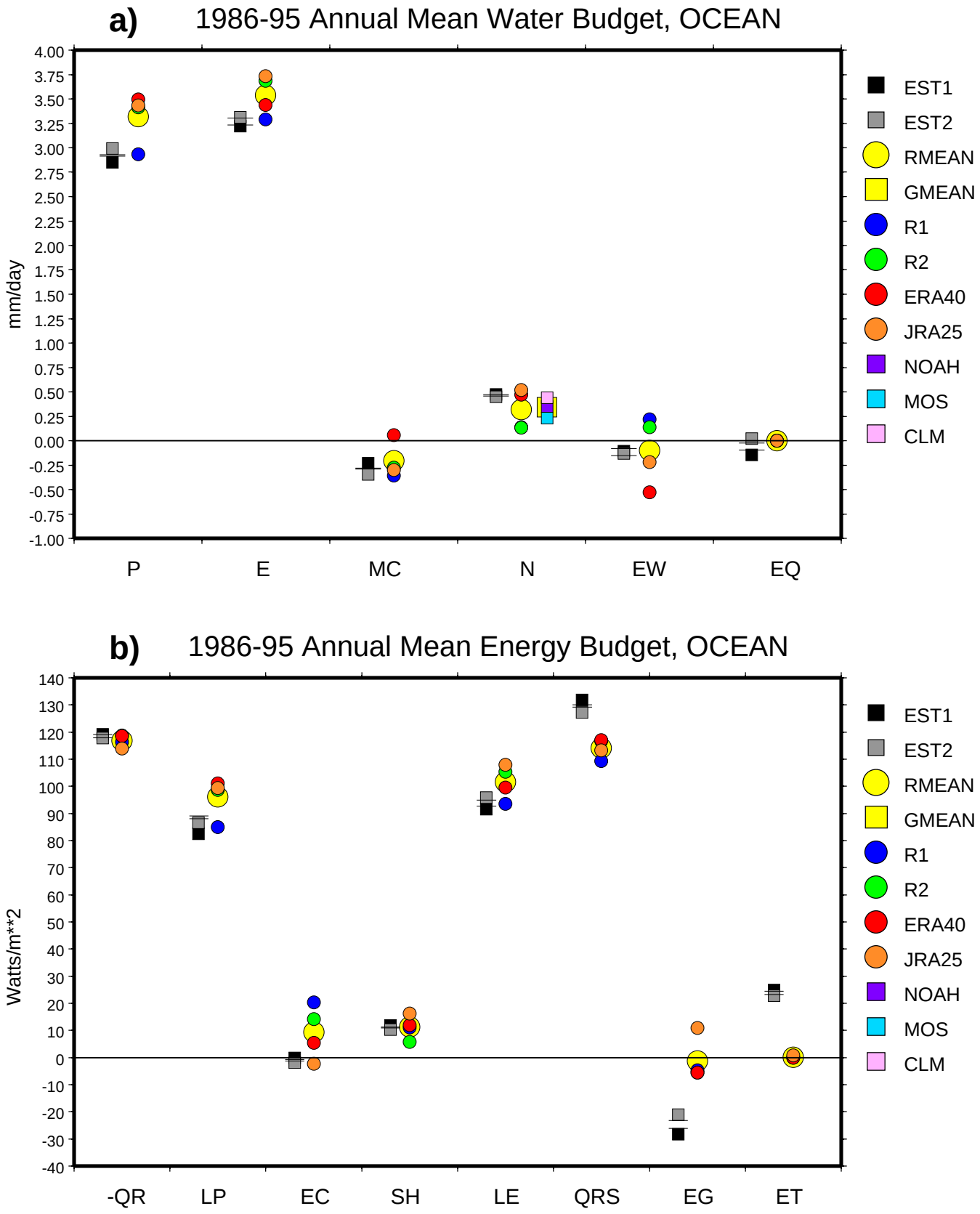
a)
1986-95 Annual Mean Water Budget, OCEAN
mm/day
4.00
3.75
3.50
3.25
3.00
2.75
2.50
2.25
2.00
1.75
1.50
1.25
1.00
0.75
0.50
0.25
0.00
-0.25
-0.50
-0.75
-1.00
P
E
MC
N
EW
EQ
EST1
EST2
RMEAN
GMEAN
R1
R2
ERA40
JRA25
NOAH
MOS
CLM
b)
1986-95 Annual Mean Energy Budget, OCEAN
Watts/m**2
140
130
120
110
100
90
80
70
60
50
40
30
20
10
0
-10
-20
-30
-40
-QR
LP
EC
SH
LE
QRS
EG
ET
EST1
EST2
RMEAN
GMEAN
R1
R2
ERA40
JRA25
NOAH
MOS
CLM

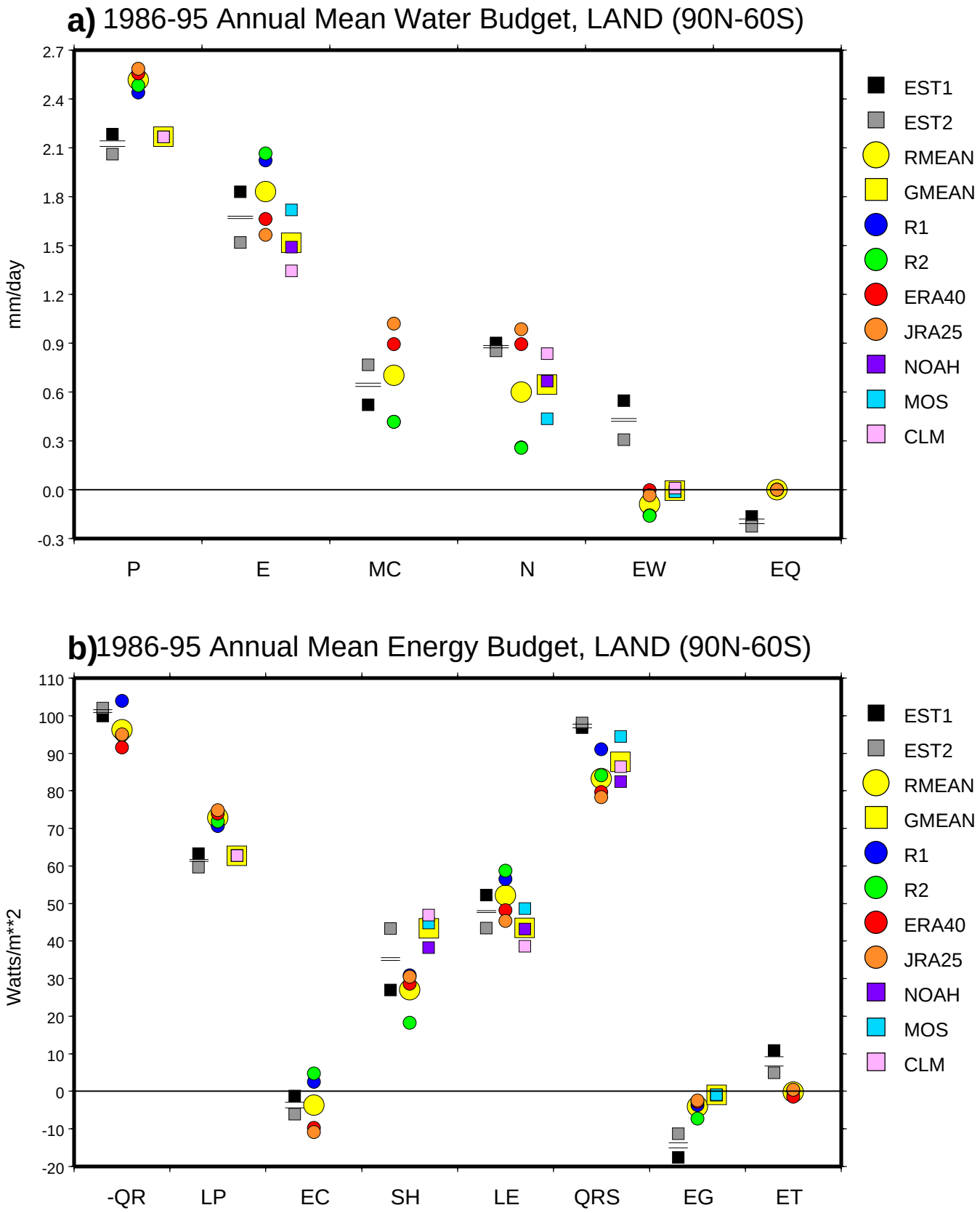
a) 1986-95 Annual Mean Water Budget, LAND (90N-60S)
mm/day
2.7
2.4
2.1
1.8
1.5
1.2
0.9
0.6
0.3
0.0
-0.3
P
E
MC
N
EW
EQ
EST1
EST2
RMEAN
GMEAN
R1
R2
ERA40
JRA25
NOAH
MOS
CLM
b) 1986-95 Annual Mean Energy Budget, LAND (90N-60S)
Watts/m**2
110
100
90
80
70
60
50
40
30
20
10
0
-10
-20
-QR
LP
EC
SH
LE
QRS
EG
ET
EST1
EST2
RMEAN
GMEAN
R1
R2
ERA40
JRA25
NOAH
MOS
CLM

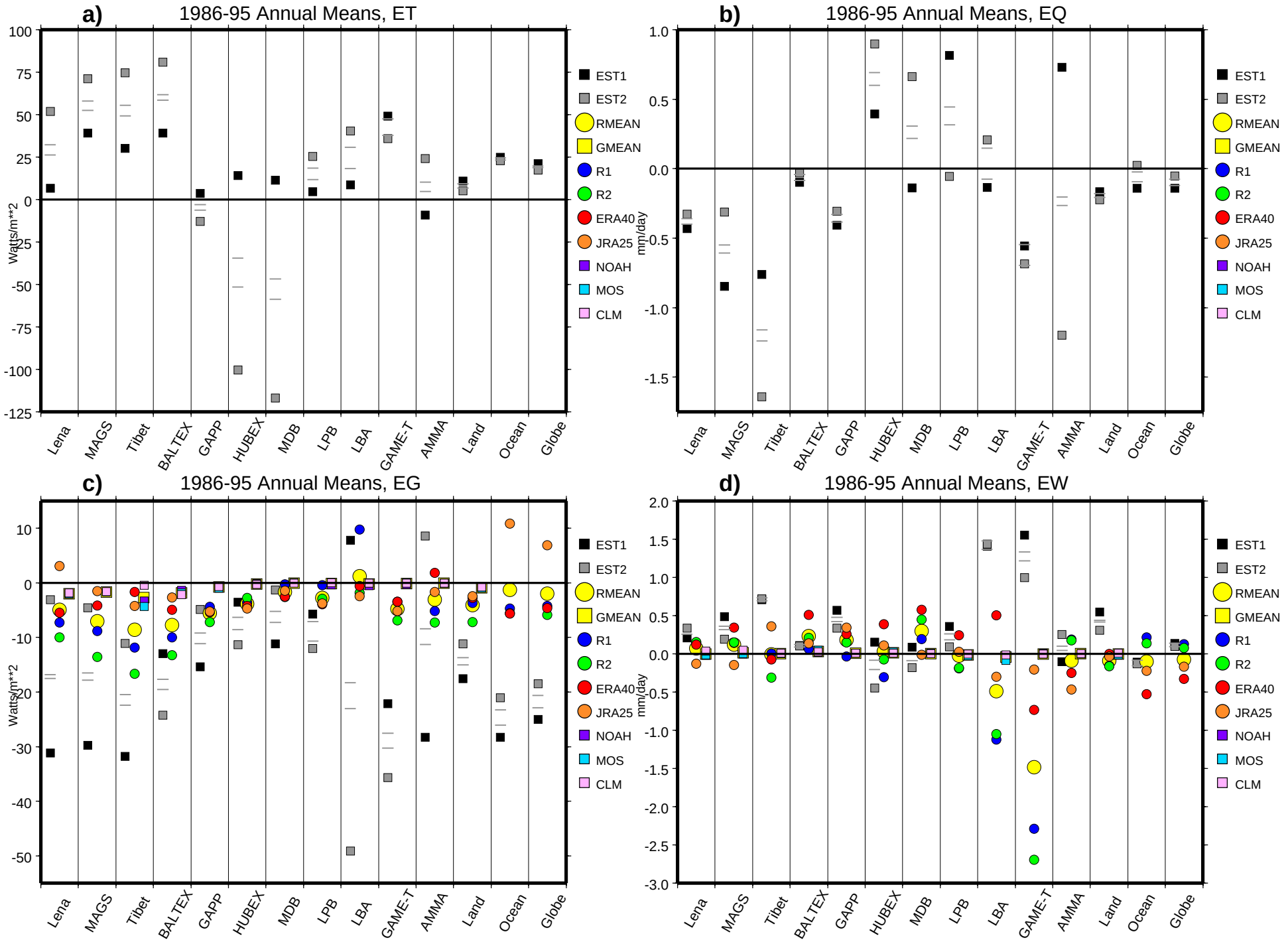
a)
1986-95 Annual Means, ET
Watts/m**2
b)
1986-95 Annual Means, EQ
mm/day
c)
1986-95 Annual Means, EG
Watts/m**2
d)
1986-95 Annual Means, EW
mm/day
EST1
EST2
RMEAN
GMEAN
R1
R2
ERA40
JRA25
NOAH
MOS
CLM
Lena
MAGS
Tibet
BALTEX
GAPP
HUBEX
MDB
LPB
LBA
GAME-T
AMMA
Land
Ocean
Globe

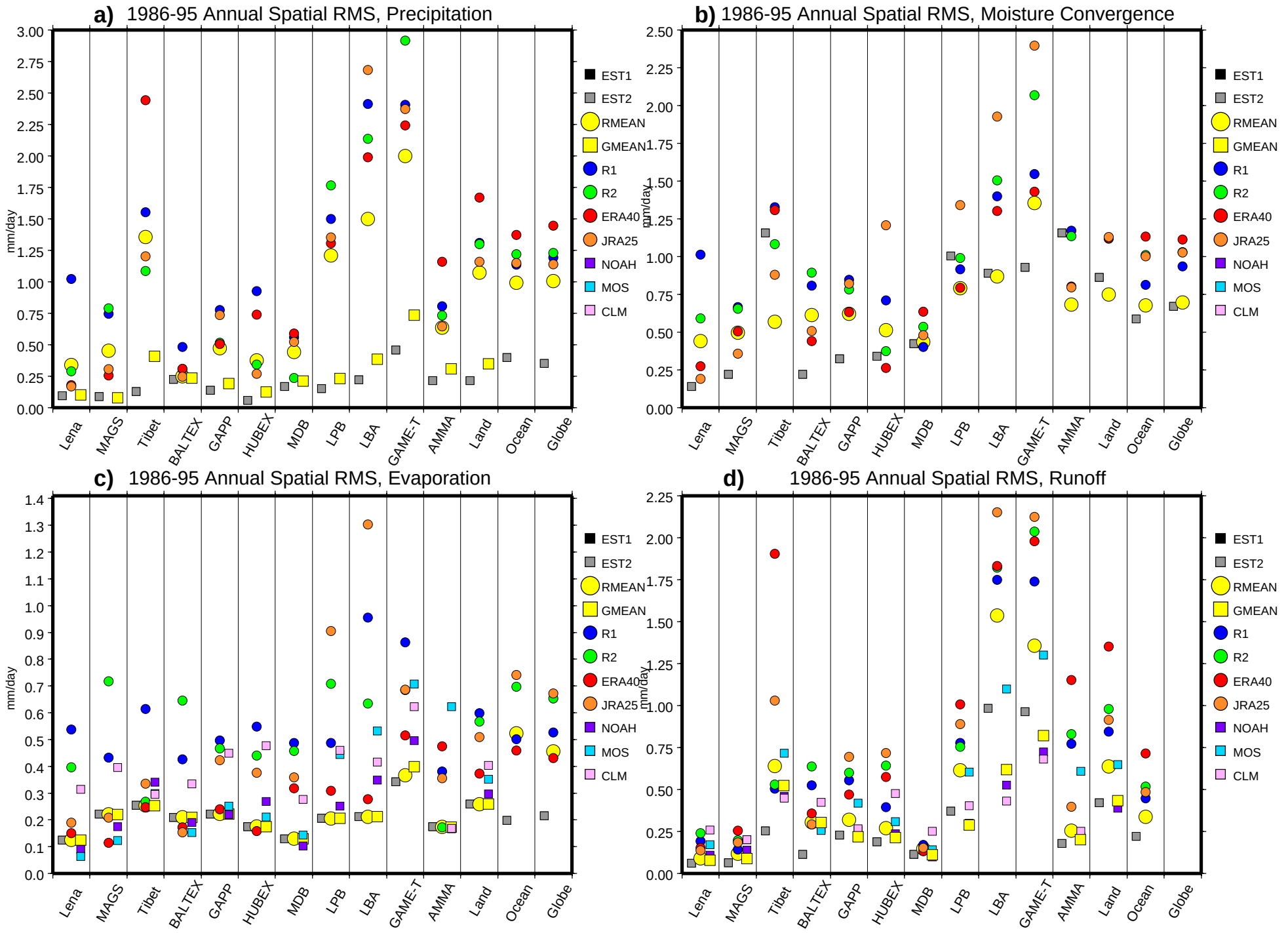
a) 1986-95 Annual Spatial RMS, Precipitation
b) 1986-95 Annual Spatial RMS, Moisture Convergence
c) 1986-95 Annual Spatial RMS, Evaporation
d) 1986-95 Annual Spatial RMS, Runoff
mm/day
EST1
EST2
RMEAN
GMEAN
R1
R2
ERA40
JRA25
NOAH
MOS
CLM
Lena
MAGS
Tibet
BALTEX
GAPP
HUBEX
MDB
LPB
LBA
GAME-T
AMMA
Land
Ocean
Globe

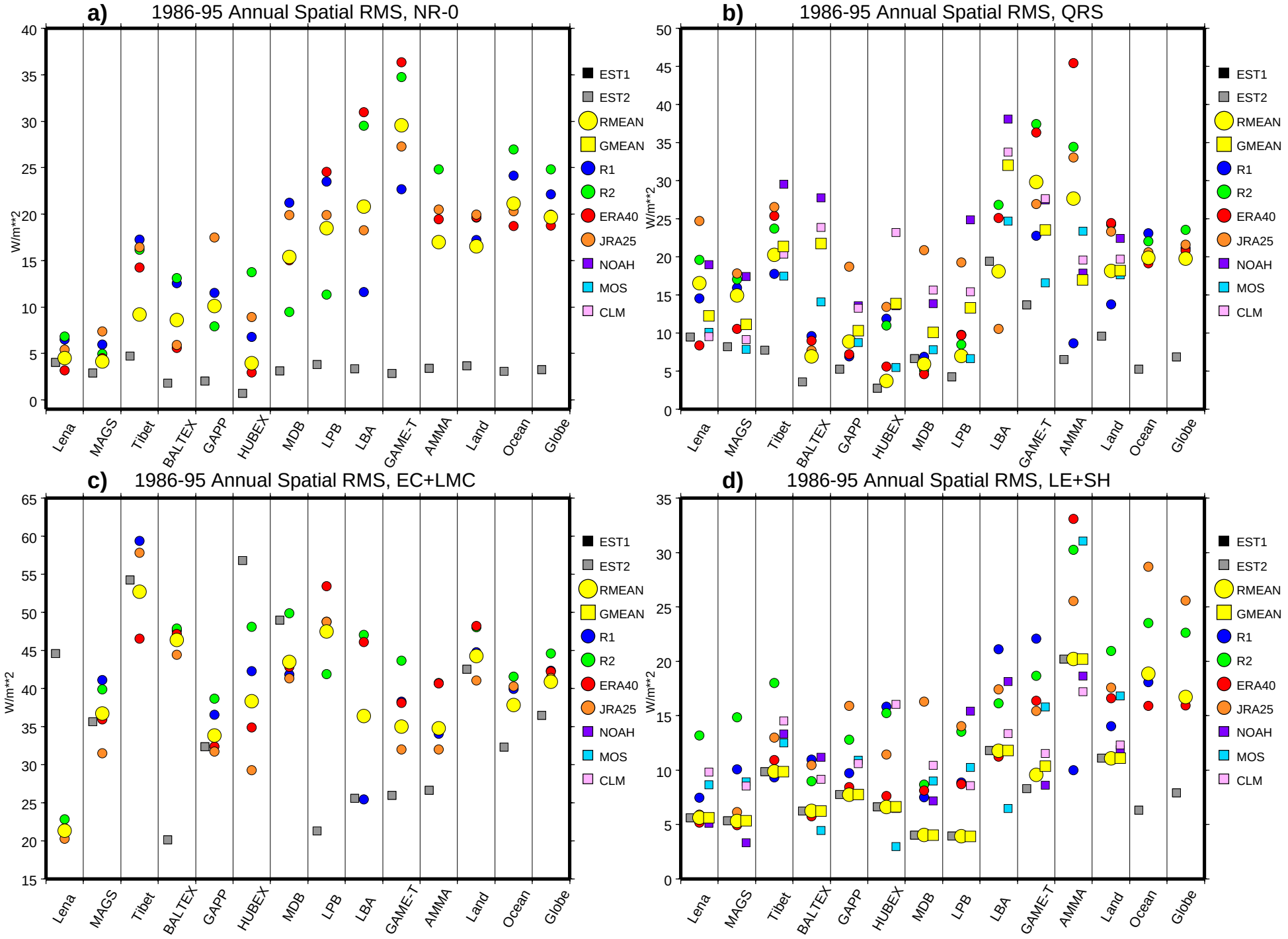
a)
1986-95 Annual Spatial RMS, NR-0
b)
1986-95 Annual Spatial RMS, QRS
c)
1986-95 Annual Spatial RMS, EC+LMC
d)
1986-95 Annual Spatial RMS, LE+SH
W/m**2
EST1
EST2
RMEAN
GMEAN
R1
R2
ERA40
JRA25
NOAH
MOS
CLM
Lena
MAGS
Tibet
BALTEX
GAPP
HUBEX
MDB
LPB
LBA
GAME-T
AMMA
Land
Ocean
Globe